Spring 2019

Mambu-RAM: a mud-aided random access MAC for underwater networks

Bryan Ehlers
University of Iowa

MAMBU-RAM: A MUD-AIDED RANDOM ACCESS MAC FOR UNDERWATER NETWORKS

by

Bryan Ehlers

A thesis submitted in partial fulfillment of the
requirements for the Master of Science
degree in Electrical and Computer Engineering in the
Graduate College of The
University of Iowa

May 2019

Thesis supervisor: Assistant Professor Ananya Sen Gupta

ACKNOWLEDGMENTS

I would like to thank my sponsor, Massachusetts Institute of Technology Lincoln Laboratory, for providing funding for this work. Also, thank you to Dr. Rachel Learned who provided many comments and time while guiding this work in a meaningful direction.

This work is partially funded by Air Force Contract No. FA8721-05-C-0002 and/or FA8702-15-D-0001, and Office of Naval Research ocean acoustics program (grant no. N00014-18-1-2081). Any opinions, findings and conclusions or recommendations expressed in this material are those of the authors and do not necessarily reflect the views of the United States Government. I would also like to profusely thank Dr. Rachel Learned of MIT Lincoln Laboratory for her comments and time.

PUBLIC ABSTRACT

The following report considers a multi-beam directional network where nodes have linear arrays capable of performing digital beamforming. Digital beamforming has greatly advanced the feasibility of uncoordinated random access in directional networks. Unlike its analog counterpart, digital beamforming alleviates the need for complex beam scheduling algorithms. A key tradeoff in such systems is the number of transducers and the network throughput. In many practical scenarios of interest, the addition of many transducers is not possible due to size weight and power (SWaP) constraints. In this work, we show for SWaP constrained nodes, the addition of a linear multiuser detector (MUD) can be utilized to further increase the throughput. It is also discussed how the varying number of chips could be used in an adaptive fashion to achieve the maximum possible throughput. Lastly, considerations of other MUD receivers are introduced along with possible further improvements such as power control.

TABLE OF CONTENTS

Page

LIST OF FIGURES vi

CHAPTER

1 INTRODUCTION 1

1.1 Background 1
1.2 System Model 3
1.3 Multi-Beam Uncoordinated Random Access MAC (MB-URAM) Policy 7

2 MAMBU-RAM MODEL 11

2.1 Enhancing MB-URAM With Multiuser Detection: MUD Aided Multi-Beam Uncoordinated Random Access MAC 11
2.2 System Model 12
2.3 Matched Filter 15
2.4 Decorrelating Detector 18
2.5 Applicability To Underwater Networks 21

3 RESULTS 28

3.1 Performance Characterization 28
3.2 MB-URAM Results 29
3.3 MAMBU-RAM Results 31
3.4 Underwater Channel 38
3.5 Underwater Channel Equalization 42

4 CONCLUSION 48

5 BIBLIOGRAPHY 50

LIST OF FIGURES

Figure Page

1.1 Example simulation layout of 30 nodes. The nodes are distributed throughout a circle according to a homogeneous Poisson point process of radius 100 meters. We consider centrally located red node when computing average link throughput. 4
1.2 Example layout of multiple nodes with randomly chosen orientation of their linear arrays. 5
1.3 Example of a 4-element array orientation (elements represented by red dots). The array's angle Θ is generated randomly for every node in every simulation run with $\Theta \sim U(0, 359)$ degrees according to a discrete uniform distribution. Every node will have an independent angle for each node's array orientation. 6
1.4 State machine for a node operating under the MB-URAM policy. The nodes are uncoordinated so that each node transitions between states independently of other nodes. That is, each node is operating on its own clock. 8
1.5 Node state time evolution for different values of the parameter x. The larger values of x means that a node will transmit with higher probability and when a listening state is chosen, it will last longer. Likewise, for smaller values of x, a node will enter the listening state with higher probability and will remain listening for a shortened amount of time. Because of this, smaller values of x results in many bursts where a node toggles more frequently between states. 10
2.1 Example signals to illustrate the asynchronous nature of the transmissions. During this time frame, the signal of interest decides to transmit and then go back to listening mode whereas the interference decides to transmit in two consecutive time slots. The receiver is assumed to perform perfect packet synchronization to acquire timing information for the signals and only considers the region in the red box for processing. 16
2.2 Simulated underwater acoustic channel with 20-meter water depth. The transmitter and receiver are set at 10-meters high at 200-meters apart. This simulates a shallow water scenario with significant interference due to reflections from the ocean surface or sea bottom. It is difficult to recover the direct-path signal in this situation because there are less reflections and thus the absorption of the signal is much less causing larger magnitude delay spread in the node-to-node channel. 25

2.3 Simulated underwater acoustic channel with 20-meter water depth. The transmitter and receiver are set at 10-meters high at 1000-meters apart. This simulates a shallow water scenario with low multipath interference that is most compatible with our method, which is designed to mitigate node-to-node interference rather than multipath interference. Because of the shallow water depth and long-range distance between the transmitter and receiver, it takes longer and more reflections, and hence more energy absorption, for the multipath arrivals to reach the receiver. 26
2.4 Simulated underwater acoustic channel with 60-meter water depth. The transmitter and receiver are set at 50-meters high at 1000-meters apart. This simulates a deep-water scenario with very weak and separable interference due to reflections from the surface or sea bottom. 27
3.1 Central nodes average throughput of MB-URAM with the matched filter receiver. From [6] we know that the parameter x ultimately limits the throughput by (x-1)/x. That is, for x=10 the best MB-URAM can achieve is 90% of the maximum throughput. But, with realistic power loss and interference introduced here, we see that the throughput is instead limited by increasing number of nodes in the network. This simulation is for SNR = 5 dB, 20 symbols per packet, 1 chip per symbol, 4 transducers, and allowing a single packet to be transmitted at a time. 30
3.2 Effect of varying the number of chips per symbol (cps) on the central nodes average throughput. As the number of nodes in the network increases, we see the MUD receivers outperforming the MF for the same number of cps. Further, for more than 20 nodes in the network, we see that the 16 cps MUD is greater than the 8 cps MF and at 30 nodes the 8 cps MUD matches the 4 cps MF receiver. But throughout, it is the 1 cps MF is still greater than any MUD with > 1 cps. This simulation is for SNR = 5 dB, x = 10, packet size of 20 symbols, 4 transducers, chip rate of 4 Kcps, transmitting one packet at a time, and varying the number chips per symbol. 34
3.3 Effect of varying the number of chips per symbol (cps) on the central nodes average throughput while allowing transmitting nodes to send two simultaneous packets. In all cases, we see that allowing simultaneous packets to be sent decreases the throughput compared to the single packet transmitting case in Figure 3.2. It is important to note that the additional chips per symbol makes the decrease in performance less severe. The 1 cps system suffers greatly, but the 4 cps system experiences less of a decrease and past 15 nodes in the network, we see the 4 cps MUD outperforming all others. This simulation is for SNR = 5 dB, x = 10, packet size of 20 symbols, 4 transducers, chip rate of 4 Kcps, transmitting two simultaneous packets at a time, and varying the number chips per symbol. 35

3.4 Effect of varying number of transducers on the central node's average throughput. For systems with higher number of transducers the beamwidth will be narrower and be better able to discriminate between tightly spaced transmitters. The system with 1 cps stands to benefit the most from additional transducers. This simulation was for a $SNR = 5$ dB, x = 10, packet size of 20 symbols, 4 chips per symbol, and variable number of transducers. The network area is $\pi 100^2$ square meters. 36
3.5 Effect of varying the number of transducers on the central nodes average throughput. As the number of transducers is increased, a node will form a narrower beam giving an increased ability to discriminate between tightly spaced transmitters. Based on this figure, it can be seen that an additional 2 receive elements gives approximately the same increase in throughput as the MUD decorrelating receiver. For example, the MUD receiver with 4 transducers traces the curve of the MF receiver with 6 transducers. This simulation is for SNR = 5 dB, x = 10, packet size of 20 symbols, 4 transducers, 4 chips per symbol, chip rate of 4 Kcps, transmitting one simultaneous packet at a time, and varying the number chips per symbol. 37
3.6 Effect of varying the number of chips per symbol (cps) on the central nodes average throughput. This simulation is for SNR = 5 dB, x = 10, packet size of 20 symbols, 4 transducers, chip rate of 4 Kcps, transmitting one packet at a time, path loss of $\frac{1}{r^3}$, and varying the number chips per symbol. 38
3.7 Effect of varying the number of chips per symbol (cps) on the central nodes average throughput while allowing transmitting nodes to send two simultaneous packets. This simulation is for SNR = 5 dB, x = 10, packet size of 20 symbols, 4 transducers, chip rate of 4 Kcps, transmitting two simultaneous packets at a time, path loss of $\frac{1}{r^3}$, and varying the number chips per symbol. 39
3.8 Effect of varying number of transducers on the central node's average throughput. For systems with higher number of transducers the beamwidth will be narrower and be better able to discriminate between tightly spaced transmitters. This simulation was for a $SNR = 5$ dB, x = 10, packet size of 20 symbols, 4 chips per symbol, transmitting one beam at a time, path loss of $\frac{1}{r^3}$, and variable number of transducers. The network area is $\pi 100^2$ square meters with 10 nodes. 40
3.9 Effect of varying the number of transducers on the central nodes average throughput. As the number of transducers is increased, a node will form a narrower beam giving an increased ability to discriminate between tightly spaced transmitters. This simulation is for SNR = 5 dB, x = 10, packet size of 20 symbols, 4 transducers, 4 chips per symbol, chip rate of 4 Kcps, transmitting one simultaneous packet at a time, path loss of $\frac{1}{r^3}$, and varying the number chips per symbol. . 41

3.10 Underwater channel equalization simulation setup. A realistic three tap underwater channel was generated to obtain the parameters. The noise variance was calculated by the residual power in the channel after taking the channel taps into account. 43
3.11 Magnitude of the underwater multi-path channel used in the simulation. We deconstructed this into a three tap channel (direct arrival and two multi-path components) and the rest of the energy in the channel is used to compute the noise variance for the AWGN added at the receiver. It can be seen that the direct arrival path is approximately constant delay and strong gain. 44
3.12 MAMBU-RAM underwater channel equalization throughput results. Performance converges for large number of chips per symbol due to the cross-correlation matrix approaching identity. This simulation was done using the realistic underwater channel described above. . 45
3.13 MAMBU-RAM underwater channel equalization link outage probability results. At 1 cps, it can be seen that the traditional matched filter is almost always failing to complete a successful transmission due to multi-path components overlapping significantly in time and strong correlations between these components and the direct arrival. Increasing the number of chips per symbol, forces the correlations to decrease since the randomness in the signature sequence decreases the off-diagonal values in the cross-correlation matrix. Performance converges for MF and MUD for large number of chips per symbol. 46
3.14 Cross-correlation matrix for the MAMBU-RAM underwater channel equalization simulation for varying number of chips per symbol. It can be seen that for more chips per symbol the correlation matrix off-diagonal elements values decreases and the matrix begins to approach identity. Indeed, this is the reason that for increasing chips the performance of the traditional matched filter and decorrelator converges in the above two plots of throughput and link outage probability. . 47

CHAPTER 1
INTRODUCTION

1.1 Background

Digital beamforming has been widely used in multi-beam directional networks and has given rise to higher transmit rates and longer transmit ranges by providing power gain proportional to the number of receive elements [1]. Additionally, digital beamforming can permit receive beams to be formed to a particular transmitter without the receiver knowing where the transmitter is located [2] [3]. A random access radio frequency (RF) medium access controller (MAC) for such a directional multiple beam network has been proposed in [6]. This work characterizes the application of the RF system in [6] to enable an acoustic communication network of underwater nodes. In addition, we propose and characterize an extension to make the original technique in [6] operational across more scenarios including small clusters of beam-coincident nodes as well as dense node environments.

In traditional underwater acoustic communication via a node with multiple transducer elements, a beam would be formed by introducing phase shifts to each of the individual transducers, so that the combination forms a beam in the appropriate direction. This makes an uncoordinated MAC unrealistic because the very nature of this traditional beamforming system is that beams must be pre-planned and pre-scheduled so that transmit and receive beams are pointing in the correct direction for successful transmission and reception (link closure) to occur. This type of scheduled MAC has been investigated in prior work under the assumption that

all node transmissions and receptions are synchronized [4]. The need for nodes to be synchronized is prohibitive in scenarios where nodes do not have a shared clock or a reliable GPS reference.

In modern digital beamforming systems, the samples of the received signal taken at each receive element of the array can be processed in an adaptive fashion allowing for beams to be formed without prior knowledge of the transmitter location [5]. This type of adaptive beamforming processing enables uncoordinated MAC policies. If the receive beams can be formed without prior knowledge of the other transmitter's locations a predetermined schedule is not required for a listening node to successfully received the signal from a transmitting node. In this work, we assess an uncoordinated MAC policy for a digital beamforming system, as proposed in [6].

The primary contribution of this work is the extension of the technique in [6] to employ multiuser detection (MUD) strategies to mitigate interference between nodes that cannot be separated with adaptive beamforming. Specifically, we propose and characterize a MUD-Aided Multi-Beam Uncoordinated Random Access MAC (MAMBU-RAM) for node-dense scenarios in which co-beam transmitters are likely. The addition of multiuser detection at the individual node level increases the likelihood of successfully received packets even when packets collide.

The computational techniques developed in this work are broadly applicable to underwater wireless sensor networks where interference between nodes is a practical reality. This work is particularly attractive to environmental monitoring applications that deploy underwater sensor networks where each node is equipped with two or more transducer elements and is capable of adaptive beamforming at each receiving node.

The initial application of MAMBU-RAM assumes close-range wireless transmission without significant channel delay spread between two nodes within the underwater network. For example, this work will be relevant to assessment and mitigation of inter-node interference within a closely spaced network of underwater sensors where the direct arrival path between any two sensors significantly dominates over any multipath arrivals. As such, the proposed technique is most applicable to underwater RF networks, but may also be applied on a limited basis to deep-water underwater acoustic networks with short-range node spacing, where multipath scattering does not dominate the channel delay spread.

1.2 System Model

We consider a network consisting of N nodes, whose locations are distributed throughout a circle according to a homogeneous Poisson point process with an average of N nodes per πr^2 area, where r is the radius of the circular simulation environment. This is illustrated in Figure 1.1. This work assumes that all nodes can either transmit or receive at a given point in time, ie. half-duplex. We do not allow a single node to transmit and receive at the same time.

Each node is equipped with a linear array. This is illustrated in Figure 1.2. To model the problem in this way is to say that some node will benefit or suffer depending on the orientation of each node's array. The orientation of each array is randomly generated by assigning each an angle $\Theta \sim U(0, 359)$ degrees according to a discrete uniform distribution, with probability mass function $P(\Theta = \theta) = \frac{1}{360}$. The nodes towards the broadside of an array will benefit from a tighter beam than those nodes towards end fire. Figure 1.3 shows an example of how a node's array angle affects its placement.

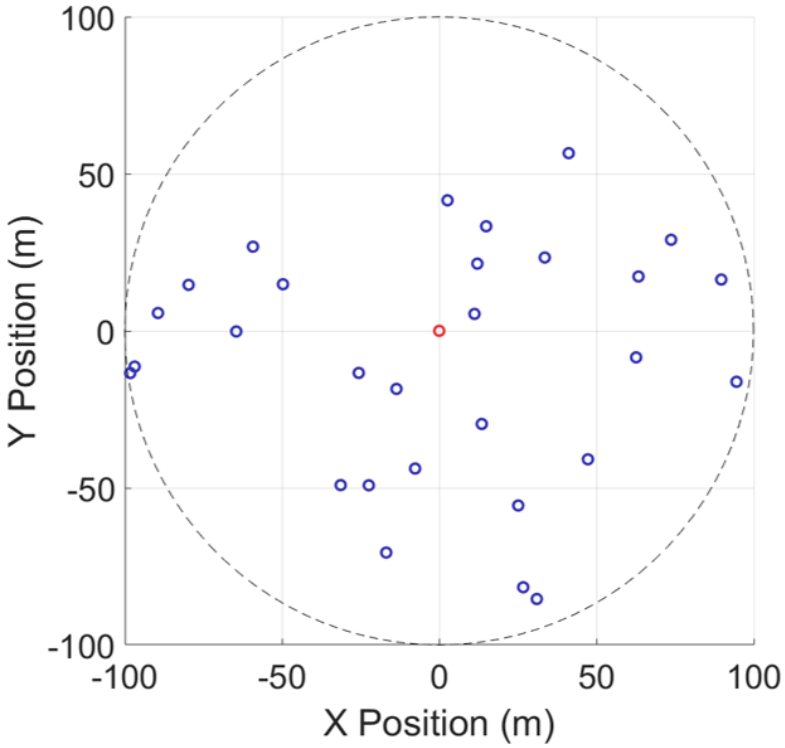

Figure 1.1: Example simulation layout of 30 nodes. The nodes are distributed throughout a circle according to a homogeneous Poisson point process of radius 100 meters. We consider centrally located red node when computing average link throughput.

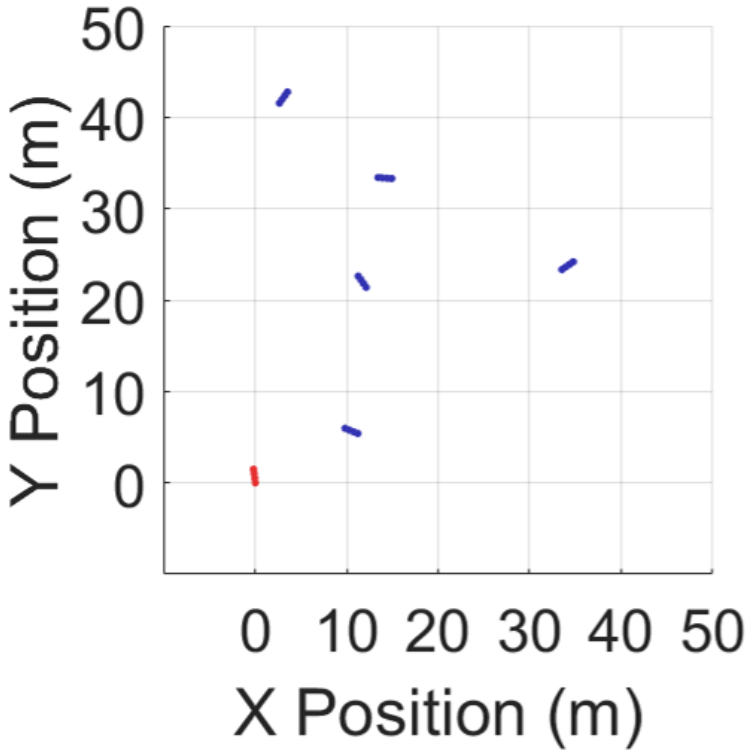

Figure 1.2: Example layout of multiple nodes with randomly chosen orientation of their linear arrays.

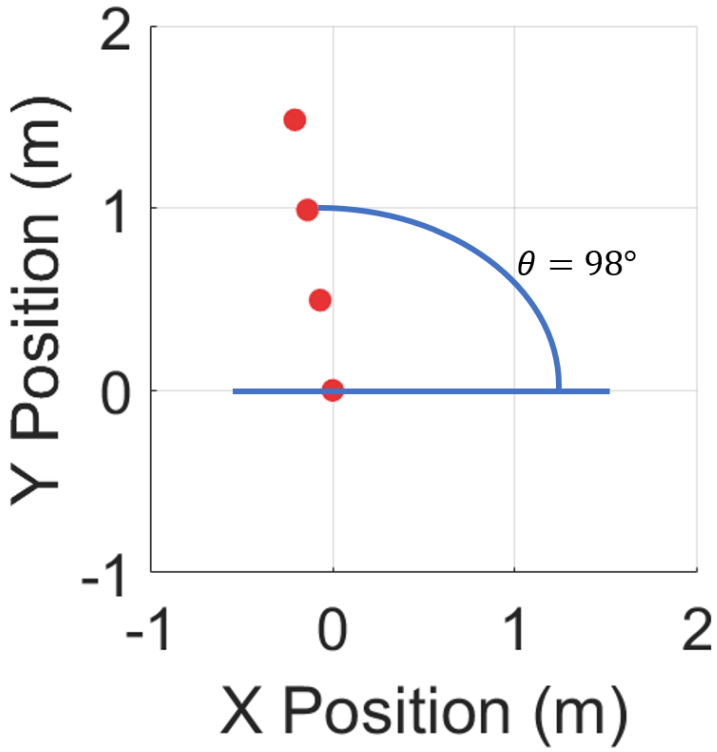

Figure 1.3: Example of a 4-element array orientation (elements represented by red dots). The array's angle Θ is generated randomly for every node in every simulation run with $\Theta \sim U(0, 359)$ degrees according to a discrete uniform distribution. Every node will have an independent angle for each node's array orientation.

The effectiveness of our proposed scheme is measured by the average throughput of the centrally located node (averaged over all packet transmissions and all randomly chosen node lay downs across all simulations. We use the term node throughput as the measure of the number of packets successfully transmitted by the node (and received by the intended destination nodes) per unit time. [1] We show how to compute this metric by example. For a given simulation setup, if node A successfully transmitted 100 packets to node B and another 100 packets to node C during a one second time block, the throughput for A node would be 200 packets/s. If the node A was able to successfully transmit 200 packets/s, 150 packets/s, and 220 packets/s over three simulation runs (every simulation run consists of generating a new node layout) then we say that the average node throughput for node A is $\frac{200+150+220}{3} = 190$ packets/s.

1.3 Multi-Beam Uncoordinated Random Access MAC (MB-URAM) Policy

The multi-beam network characterized in this paper is one in which each node is equipped with an M-element uniform linear array with half wavelength spaced elements. For any real system, a maximum transmit power constraint will need to be set, ultimately limiting the number of simultaneous transmissions to different receivers located at different lines of bearing, one beam for each. We consider nodes with a per beam transmit power of P_B and maximum number of allowable beams to be N_B, resulting in a maximum transmit power for the array, $P_B N_B$. During our simulations, we use both $N_B = 1$ and $N_B = 2$ beams. Regardless of the number of nodes in the network, it is assumed that the receiving node is able to form a

[1] Equivalently, throughput may also be expressed in terms of bits/unit of time. To map packets/unit of time to bits/unit of time, we need only know the number of bits/packet.

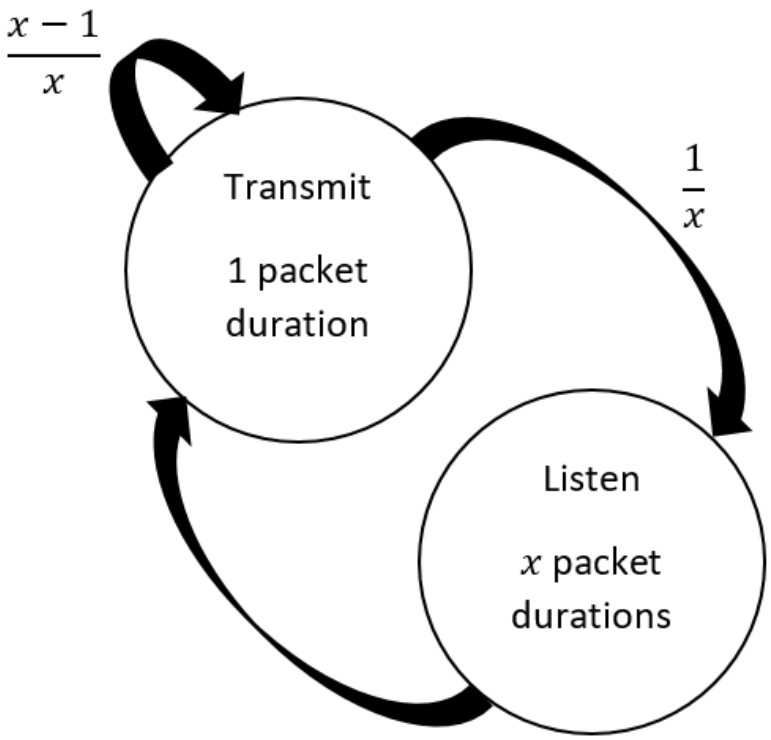

Figure 1.4: State machine for a node operating under the MB-URAM policy. The nodes are uncoordinated so that each node transitions between states independently of other nodes. That is, each node is operating on its own clock.

sufficient number of beams to attempt to receive all incoming packets. In the event two transmitting nodes are located within a single receive beam, the single band version of the system of [6] cannot successfully transmit packets to both receivers at the same time because there is no mechanism in place at the receivers to mitigate the interference that results from transmitting two different signals in the same frequency band at the same time in the same direction.

Following the policy adopted in Kuperman et. al. [6], each MB-URAM node behaves as follows: when a node is set to transmit, it transmits to a maximum of M nodes. Each transmission is done by forming a beam in the direction of the intended receiver. Each beam that a transmitter form can potentially carry independent information. After a node is done transmitting, it chooses with probability $\frac{x-1}{x}$ to transmit again, and chooses with probability $\frac{1}{x}$ to go to listening state for x packet durations. More specifically, Figure 1.4 shows the operation of a typical node using the MB-URAM policy. After a node is done transmitting, either it will choose to transmit again with probability $\frac{x-1}{x}$ or it will go to a listening state for x packet durations with probability $\frac{1}{x}$. When a node is in transmit state, it will remain for one packet duration and when in listening state, it will remain for x packet durations. This behavior is summarized pictorially in Figure 1.4. The parameter x, therefore, governs the packet transmission behavior of a node. Figure 1.5 shows the activity of a typical node operating under the MB-URAM policy. From this, it is clear that varying the parameter x controls how often a node transmits packets to the channel and how long a node is in listening state. The higher the value of x, the higher the probability that a node will transition to transmitting mode, and when a node goes into listening mode the longer the node will stay in listening mode.

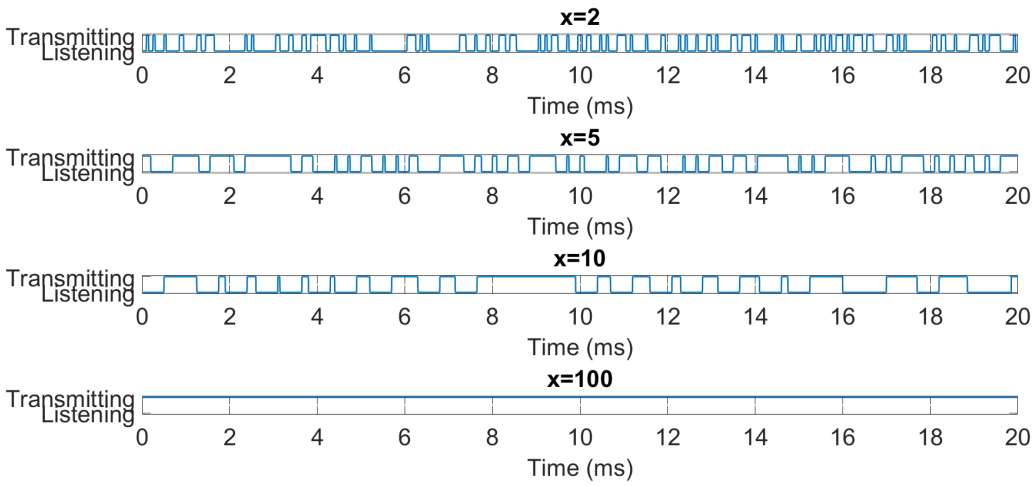

Figure 1.5: Node state time evolution for different values of the parameter x. The larger values of x means that a node will transmit with higher probability and when a listening state is chosen, it will last longer. Likewise, for smaller values of x, a node will enter the listening state with higher probability and will remain listening for a shortened amount of time. Because of this, smaller values of x results in many bursts where a node toggles more frequently between states.

CHAPTER 2
MAMBU-RAM MODEL

2.1 Enhancing MB-URAM with Multiuser Detection: MUD Aided Multi-Beam Uncoordinated Random Access MAC

As we saw in the previous section, and as is the case in all deployed wireless networks, significant degradation in throughput results when the number of nodes is large. The degradation in the case of the MB-URAM system characterized above was due to the existence of more than one nearby transmitter in the same beam. In this case, the MB-URAM receiving node cannot mitigate the interfering signals and therefore drops the one or more colliding packets that were meant for that node. One way to combat this is to increase the number of antenna elements at each node so as to make the beams narrower, making it less likely for multiple transmitters to co-exist in a single narrow beam. This solution is of limited appeal since with each new antenna element comes additional receiver hardware, causing significant increase in size, weight and power. A second approach to combat the interference problems was to introduce the ability to transmit over multiple non-interfering frequency bands and a frequency division multiple access (FDMA) approach was outlined [6].

Instead of relying on additional frequency bands and the need for a coordinated FDMA overlay scheme, we propose mitigating instances of two or more interfering signals in a single beam with receiver processing designed to pull apart co-channel interfering signals, namely, multiuser detection (MUD). We call the resulting scheme

a MUD-Aided MB-URAM (MAMBU-RAM). In this work, we employ the decorrelator MUD [8] [10] to mitigate interference between the signals from co-beam interfering nodes. The practical consequence is that by using a more sophisticated processing at the receiver, the system will successfully support more transmitters per beam and increase the throughput.

MAMBU-RAM has the potential to greatly improve networks when the size or weight of nodes must be constrained and therefore the number of antenna elements must be small. In the next section, a basic synchronous and asynchronous model is introduced followed by an outline of the matched filter and decorrelating detector.

2.2 System Model

We begin by defining the synchronous multiuser scenario before moving on to the necessary asynchronous model for our work. Consider a typical scenario, there are K transmitter communicating to a single receiver. The k^{th} transmitter's received signal at a node that has already formed a beam is of the form:

$$y(t) = \sqrt{\alpha_k g_k E_k} b_k s_k(t) + w(t), t \in [0, T] \tag{2.1}$$

where $\alpha_k, g_k, E_k, b_k, s_k(t)$, and T are the propagation power loss, beam-gain, transmit power, symbol, signature waveform, and symbol period of the k^{th} transmitting transmitter respectively. The baud rate is then $\frac{1}{T}$. Each transmitter's signature waveform is chosen at random to be a generic direct sequence spread spectrum signature that is generated by N_c successive pulses, where each pulse is multiplied by a 1 or -1 according to pseudonoise (PN) sequences of length N_c [7]. We apply a simple power loss of $\alpha_i = \frac{1}{r_k^3}$ [26], where r_k is the distance between the k^{th} transmitter and centrally located receiver. It is assumed that the receiver noise $w(t)$ is a Gaussian process with zero mean and variance of σ^2. The aggregate received continuous time

signal is comprised of all K transmitted signals:

$$y(t) = \sum_{k=1}^{K} \sqrt{\alpha_k g_k E_k} b_k s_k(t) + w(t), t \in [0, T] \tag{2.2}$$

Further, the discrete time signal sampled at a sufficient sampling interval T_s is:

$$\begin{aligned} y[n] &= \sum_{k=1}^{K} \sqrt{\alpha_k g_k E_k} b_k s_k(nT_s) + w[n] \\ &= \sum_{k=1}^{K} A_k b_k s_k(nT_s) + w[n] \end{aligned} \tag{2.3}$$

Or, in vector notation:

$$\mathbf{y} = \mathbf{SAb} + \mathbf{w} \tag{2.4}$$

where $\mathbf{A} \in \mathbb{R}^{K \times K}$ is a diagonal matrix containing the the received amplitudes

$$A_k = \sqrt{\alpha_k g_k E_k} \tag{2.5}$$

each corresponding to a post-beamformed received packet. Received signal amplitude and received signal power are simply related where the received signal power of the k^{th} packet from the k^{th} transmitter is $A_k^2 = \alpha_k g_k E_k$. The matrix $\mathbf{A}$ in Equation 2.4 becomes

$$\mathbf{A} = \begin{bmatrix} \sqrt{\alpha_1 g_1 E_1} & 0 & 0 & \dots & 0 \\ 0 & \sqrt{\alpha_2 g_2 E_2} & 0 & \dots & 0 \\ \vdots & \vdots & \vdots & \ddots & \vdots \\ 0 & 0 & \dots & \dots & \sqrt{\alpha_K g_K E_K} \end{bmatrix} \tag{2.6}$$

The k^{th} column of the matrix $\mathbf{S}$ contains the sampled signature sequence used by the k^{th} transmitter. Each transmitter's sampled signature sequence is of length $\frac{N_c T_c}{T_s}$, where N_c is the number of chips and $\frac{T_c}{T_s}$ is the number of samples per chip. The matrix is scaled by $\frac{1}{\sqrt{\frac{N_c T_c}{T_s}}}$ such that each column is of unit energy, $\mathbf{s}_i^T \mathbf{s}_i = 1$.

$$\mathbf{S} = \frac{1}{\sqrt{\frac{N_c T_c}{T_s}}} \begin{bmatrix} s_1[1] & s_2[1] & \dots & s_K[1] \\ s_1[2] & s_2[2] & \dots & s_K[2] \\ \vdots & \vdots & \ddots & \vdots \\ s_1[\frac{N_c T_c}{T_s}] & s_2[\frac{N_c T_c}{T_s}] & \dots & s_K[\frac{N_c T_c}{T_s}] \end{bmatrix} \tag{2.7}$$

For the synchronous scenario, the above formulation holds because such a system is symbol synchronous. That is, transmitter 1's received symbol is overlapping in time with the other $(K-1)$ transmitter's symbols. Next, we turn our attention to the asynchronous case which is what a receiver will experience when operating under the random access scheme from [6].

For an uncoordinated random access scenario, a typical receiver is receiving from K transmitters each having a random timing offset, and Equation 2.2 becomes:

$$y(t) = \sum_{k=1}^{K} A_k b_k s_k(t - \tau_k) + w(t), t \in [0, T] \tag{2.8}$$

where τ_k is the k^{th} transmitter's timing offset. Without loss of generality, it can be assumed that $\tau_1 \leq \tau_2 \leq \cdots \leq \tau_K$. The sampled asynchronous received signal is:

$$y[n] = \sum_{k=1}^{K} A_k b_k s_k(nT_s - d_k) + w[n] \tag{2.9}$$

The discrete time delays for each packet, d_i, can be expressed in terms of samples, so the delays are such that $d_i \in \{0, 1, \dots, \frac{N_s N_c T_c}{T_s} - 1\}$, where N_s is the number of symbols per packet. The corresponding asynchronous vector model is obtained by substituting the delay-incorporating version of $\mathbf{S}$ into Equation 2.4.

To solidify how the delays are applied, suppose for $K = 2$, we have $d_1 = 1$ samples and $d_2 = 3$ samples. Then, for a packet with only two symbols [1], the

[1] Packets typically contain hundreds to thousands of symbols, but for ease of understanding, we show an example with only two symbols per packet.

signature matrix is given by:

$$\mathbf{S} = \frac{1}{\sqrt{\frac{N_c T_c}{T_s}}} \begin{bmatrix} 0 & 0 & 0 & 0 \\ s_1[1] & 0 & \vdots & \vdots \\ \vdots & 0 & \vdots & \vdots \\ \vdots & s_2[1] & \vdots & \vdots \\ \vdots & \vdots & \vdots & \vdots \\ s_1[\frac{N_c T_c}{T_s}] & \vdots & 0 & \vdots \\ 0 & \vdots & s_1[1] & \vdots \\ \vdots & s_2[\frac{N_c T_c}{T_s}] & \vdots & 0 \\ \vdots & 0 & \vdots & s_2[1] \\ \vdots & \vdots & \vdots & \vdots \\ \vdots & \vdots & s_1[\frac{N_c T_c}{T_s}] & \vdots \\ \vdots & \vdots & 0 & \vdots \\ 0 & 0 & 0 & s_2[\frac{N_c T_c}{T_s}] \end{bmatrix} \tag{2.10}$$

For our simulation, this construction of the matrix $\mathbf{S}$ is extended for packets with more symbols and more transmitting nodes ($K > 2$). Due to the asynchronous behavior of the transmissions, partial overlaps of packets and symbols can occur. In this situation, we consider the receiver to process the signal of interest's time slot as in Figure 2.1.

2.3 Matched Filter

By passing $y(t)$ through a bank of matched filters, ie. pre-multiplying $\mathbf{y}$ by $\mathbf{S}^T$, the outputs are given in vector form as:

$$\begin{aligned} \mathbf{r} &= \mathbf{S}^T \mathbf{y} \\ &= \mathbf{S}^T (\mathbf{SAb} + \mathbf{w}) \\ &= \mathbf{RAb} + \mathbf{n} \end{aligned} \tag{2.11}$$

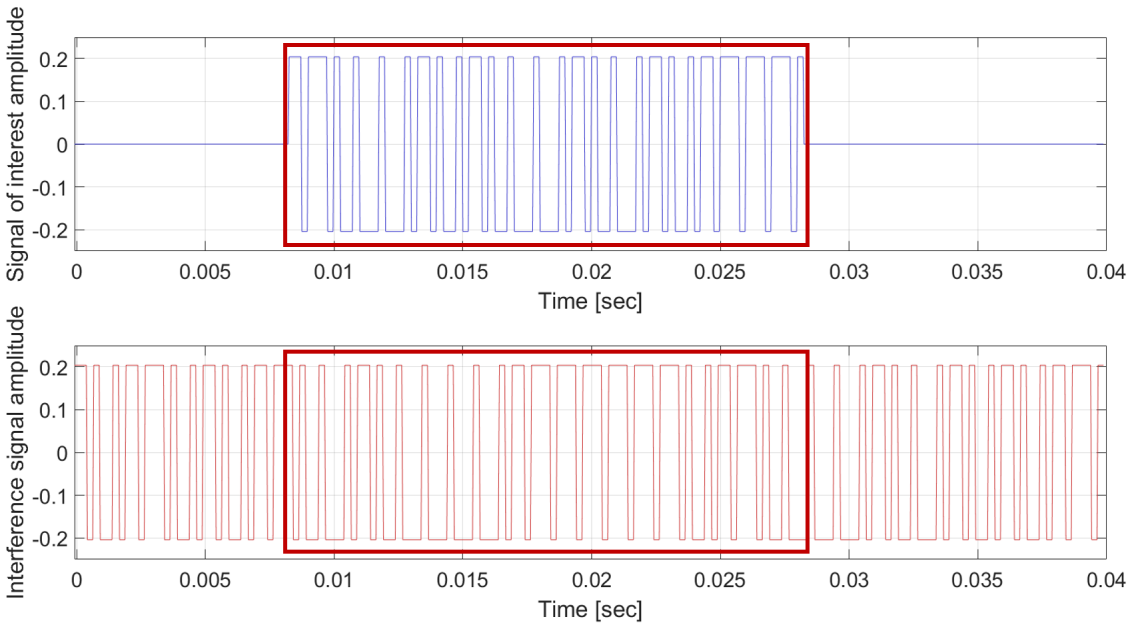

Figure 2.1: Example signals to illustrate the asynchronous nature of the transmissions. During this time frame, the signal of interest decides to transmit and then go back to listening mode whereas the interference decides to transmit in two consecutive time slots. The receiver is assumed to perform perfect packet synchronization to acquire timing information for the signals and only considers the region in the red box for processing.

where $\mathbf{R} \in \mathbb{R}^{N_s K \times N_s K}$ is the normalized partial correlation matrix, $\mathbf{R} = \mathbf{S}^T\mathbf{S}$, where N_s is the number of symbols in a packet transmission. Further, $\mathbf{b} \in \mathbb{C}^{N_s K \times 1}$ vector of the transmitted symbols, $\mathbf{n}$ is a zero mean Gaussian vector with covariance matrix $\sigma^2\mathbf{R}$, and $\mathbf{r} \in \mathbb{C}^{N_s K \times 1}$ is the vector of matched filter outputs. For simplicity, we are assuming the elements of $\mathbf{b}$, $b_i \in (-1, +1)$, for binary phase shift keying (BPSK) modulation.

To compute the SINR after the matched filtering is done, we first break up the discrete time signal model in Equation 2.4:

$$\begin{aligned} \mathbf{y} &= \mathbf{y}_{SOI} + \mathbf{y}_{INT} + \mathbf{w} \\ &= \mathbf{S}_{SOI}\mathbf{A}_{SOI}\mathbf{b}_{SOI} + \mathbf{S}_{INT}\mathbf{A}_{INT}\mathbf{b}_{INT} + \mathbf{w} \end{aligned} \tag{2.12}$$

The corresponding outputs of the matched filters can then be found as

$$\mathbf{r}_{SOI} = \mathbf{S}^T\mathbf{y}_{SOI} \tag{2.13}$$

$$\mathbf{r}_{INT} = \mathbf{S}^T\mathbf{y}_{INT} \tag{2.14}$$

$$\mathbf{r}_{w} = \mathbf{S}^T\mathbf{w} \tag{2.15}$$

This gives $\mathbf{r}_{SOI}$, $\mathbf{r}_{INT}$, and $\mathbf{r}_w$ as length $K * N_s$ vectors, where N_s is the number of symbols in a packet and K is the number of transmitters. Letting $\tilde{\mathbf{r}}_{SOI}$, $\tilde{\mathbf{r}}_{INT}$, and $\tilde{\mathbf{r}}_w$ be the matched filter outputs corresponding only to the signal of interest we can calculate the average SINR over the SOI's packet as:

$$SINR_{MF} = \frac{||\tilde{\mathbf{r}}_{SOI}||^2}{||\tilde{\mathbf{r}}_{INT}||^2 + ||\tilde{\mathbf{r}}_w||^2} \tag{2.16}$$

where, for a column vector $\mathbf{x}$ of length N, $||\mathbf{x}||^2 = x_1x_1 + x_2x_2 + \cdots + x_Nx_N$, and division is done element wise.

Due to the nature of the collisions of other packets with the SOI packet, specifically, an SOI's packet may overlap a colliding packet only partially, see Figure 2.1 for an illustration. The model for determining when an asynchronous MB-URAM node drops an SOI's packet, is more complex than simply computing the

Shannon capacity based upon the average $SINR_{MF}$ computed in Equation 2.16. Instead, we propose using a a symbol-by-symbol SINR, defined as:

$$\gamma_{MF} = \frac{\tilde{\mathbf{r}}_{SOI} \odot \tilde{\mathbf{r}}_{SOI}}{\tilde{\mathbf{r}}_{INT} \odot \tilde{\mathbf{r}}_{INT} + \tilde{\mathbf{r}}_{w} \odot \tilde{\mathbf{r}}_{w}} \tag{2.17}$$

where the operation $\odot$ is defined here as element wise multiplication. For example, for two N-element vectors $\mathbf{x}$ and $\mathbf{y}$, $\mathbf{x} \odot \mathbf{y} = [x_1 y_1, x_2 y_2, \cdots, x_N y_N]^T$. The division in Equation 2.17 is also done on an element by element basis so that the resulting γ_{MF} is a *vector* of length N_s containing the SINR for each symbol in the signal of interest's packet. Given this, we can calculate the maximum achievable rate as:

$$R_{MAX}^{MF} = \frac{1}{2} log_2 \left(1 + \gamma_{MF} \right) \tag{2.18}$$

This gives R_{MAX}^{MF} as a vector of length N_s. In a later section, we will discuss how it is used to determine whether or not a packet is dropped.

2.4 Decorrelating Detector

The decorrelating detector is a linear receiver that takes advantage of any difference between the space spanned by the received signal of interest and the space spanned by the received interfering signal or signals [8]. Analysis of the decorrelator has been done in [9] for both synchronous and asynchronous systems. Here, we focus our attention to the asynchronous model, where the decorrelating filter is given by:

$$\mathbf{F} = (\mathbf{S}^T \mathbf{S})^{-1} = \mathbf{R}^{-1} \tag{2.19}$$

The decorrelator can be seen as a bank of filters where each row of $\mathbf{F}$ is the filter for a specific transmitter and a specific symbol. It is assumed that the receiving nodes have obtained an exact copy of the true matrix $\mathbf{R}$ to do processing. Future work to

estimate $\mathbf{R}$ or $\mathbf{F}$ from the received signals is recommended and should include the characterization of estimation error effects on performance.

Assuming that $\mathbf{R}$ is invertible [2] the symbol estimates are given by:

$$\hat{\mathbf{b}} = \text{sign}(\mathbf{F}(\mathbf{RAb} + \mathbf{n})) \tag{2.20}$$

where $\hat{\mathbf{b}} \in \mathbb{C}^{K\times 1}$ vector of symbol estimates. The decorrelating detector was chosen to be a starting point for this research because it is highly amenable to implementation using today's technology and it does not require an estimate of the received amplitudes. This is unlike other detectors, such as the successive interference canceller (SIC), which requires estimates of amplitudes and can suffer if the estimates are not accurate [7]. After applying the decorrelating detector to $\mathbf{r}$, we have:

$$\mathbf{R}^{-1}\mathbf{r} = \mathbf{Ab} + \mathbf{R}^{-1}\mathbf{n} \tag{2.21}$$

which has a signal component: $\mathbf{Ab}$, and a noise component: $\mathbf{R}^{-1}\mathbf{n}$. The noise component is Gaussian, zero mean, and has a covariance matrix $\mathbf{R}^{-1}\sigma^2$. It should be noted that the effect of interference has been nulled out completely, this is why the decorrelator is also termed as the interference nulling detector. If $\mathbf{R}^{-1}$ contains large values, then the noise vector is effectively amplified by the decorrelating operation and the post-decorrelator SINR will suffer leading to a loss in performance.

To compute the SINR after applying the decorrelator, we pick up from the signal of interest, interference signal(s), and noise components at the outputs of the matched filters, ie. Equations 2.13, 2.14, and 2.15. The decorrelator is given by: $\mathbf{F} = (\mathbf{S}^T\mathbf{S})^{-1} = \mathbf{R}^{-1}$. The Moore-Penrose pseudoinverse can also be computed in place of $\mathbf{R}^{-1}$ [7]. Then the component of the signal of interest, interference signal(s),

[2] Although alternate linear MUDs exist, such as the MMSE MUD, for the case of $\mathbf{R}$ not invertible, linear MUDs generally offer poor performance in this case and should be replaced by non-linear MUDs (e.g. a decision feedback type of MUD) that take advantage of additional signal structure such as the constraints on the symbol weights [10].

and noise that get through the decorrelating filter is:

$$\mathbf{u}_{SOI} = \mathbf{F}\mathbf{r}_{SOI} \tag{2.22}$$

$$\mathbf{u}_{INT} = \mathbf{F}\mathbf{r}_{INT} \tag{2.23}$$

$$\mathbf{u}_{w} = \mathbf{F}\mathbf{r}_{w} \tag{2.24}$$

Again, $\mathbf{u}_{SOI}$, $\mathbf{u}_{INT}$, and $\mathbf{u}_w$ will be length $K * N_s$ vectors. We take only the entries corresponding to the signal of interest to get length N_s vectors $\tilde{\mathbf{u}}_{SOI}$, $\tilde{\mathbf{u}}_{INT}$, and $\tilde{\mathbf{u}}_w$.

And the power of the signal of interest, interference signal(s), and noise that made it through the signal's filter: $\tilde{\mathbf{u}}_{SOI} \odot \tilde{\mathbf{u}}_{SOI}$, $\tilde{\mathbf{u}}_{INT} \odot \tilde{\mathbf{u}}_{INT}$, and $\tilde{\mathbf{u}}_w \odot \tilde{\mathbf{u}}_w$

And the post decorrelating SINR is given as:

$$\gamma_D = \frac{\tilde{\mathbf{u}}_{SOI} \odot \tilde{\mathbf{u}}_{SOI}}{\tilde{\mathbf{u}}_{INT} \odot \tilde{\mathbf{u}}_{INT} + \tilde{\mathbf{u}}_w \odot \tilde{\mathbf{u}}_w} \tag{2.25}$$

γ_D is a length N_s vector containing the SINR for each symbol in the signal of interest's packet.

Since the transmitters closer to the central node will contribute more power than the others, it does not always make practical sense to include all the interfering transmitters in the MUD processing. For example, there may be transmitter with little power who could make $\mathbf{R}$ singular or severely ill-conditioned leading to more significant noise enhancement. For these reasons, we would prefer to ignore the lower power interfering signals in the MUD processing.

The received signal model of Equation 2.4 can be split as follows

$$\mathbf{y} = \mathbf{S}_{\mathbb{A}}\mathbf{A}_{\mathbb{A}}\mathbf{b}_{\mathbb{A}} + \mathbf{S}_{\mathbb{B}}\mathbf{A}_{\mathbb{B}}\mathbf{b}_{\mathbb{B}} + \mathbf{w} \tag{2.26}$$

where $\mathbf{S} = [\mathbf{S}_{\mathbb{A}}\mathbf{S}_{\mathbb{B}}]$ and use the following scheme to decide which interfering transmitters to include in the MUD, and thus include in $\mathbf{S}_{\mathbb{A}}$ and which to ignore and include in $\mathbf{S}_{\mathbb{B}}$. Denote the received power associated with the signal of interest as P_{SOI} and the received signal power of the j^{th} interfering signal as P_j, and compute

the SINR for the A-B sorting test for this signal pair as

$$SINR_{test} = \frac{P_{SOI}}{\sigma^2 + P_j} \tag{2.27}$$

We include the j^{th} interfering signal and corresponding columns of $\mathbf{S}$ into $\mathbf{S}_{\mathbb{A}}$ if $SINR_{test} \leq SINR_{min} + \delta$, where $SINR_{min}$ is the minimum SNR that would be needed to receive the packet at the desired rate. For our simulations we set a desired rate of 1 bit per channel use, then it is required by Equation 3.1 that the SINR be at least 3 (= 4.77 dB). For our simulations, we take $\delta = 2 = 3$ dB. If $SINR_{test} > SINR_{min} + \delta$, we move the j^{th} interfering signal and corresponding columns of $\mathbf{S}$ into $\mathbf{S}_{\mathbb{B}}$. The partial decorrelating filter bank is now

$$\mathbf{F}_{\mathbb{A}} = (\mathbf{S}_{\mathbb{A}}{}^T \mathbf{S}_{\mathbb{A}})^{-1} = \mathbf{R}_{\mathbb{A}}{}^{-1} \tag{2.28}$$

To compute the SINR that would be present after the application of the partial decorellator, we adapt Equation 2.25 to account for the signals that are not included in the MUD:

$$\gamma_{PD} = \frac{\tilde{\mathbf{u}}_{SOI} \odot \tilde{\mathbf{u}}_{SOI}}{\tilde{\mathbf{u}}_{\mathbb{A}} \odot \tilde{\mathbf{u}}_{\mathbb{A}} + \tilde{\mathbf{u}}_{\mathbb{B}} \odot \tilde{\mathbf{u}}_{\mathbb{B}} + \tilde{\mathbf{u}}_{w} \odot \tilde{\mathbf{u}}_{w}} \tag{2.29}$$

where $\tilde{\mathbf{u}}_{SOI}$, $\tilde{\mathbf{u}}_{\mathbb{A}}$, $\tilde{\mathbf{u}}_{\mathbb{B}}$, and $\tilde{\mathbf{u}}_{w}$ are the signal of interest, interference in the group the MUD considers ($\mathbb{A}$), interference in the group MUD ignores ($\mathbb{B}$), and noise components present at the outputs of this partial decorrelator, $\mathbf{F}_{\mathbb{A}}$. The highest achievable rate for the partial decorrelating receiver is then:

$$R_{PD}^{MAX} = \frac{1}{2} log_2 \left(1 + \gamma_{PD} \right) \tag{2.30}$$

2.5 Applicability To Underwater Networks

The computational techniques developed in this work are broadly applicable to underwater wireless sensor networks where interference between nodes is a practical reality. This work is particularly attractive to environmental monitoring

applications that deploy underwater sensor networks where each node is equipped with two or more transducer elements and is capable of adaptive beamforming at each receiving node.

Our theoretical setup and analysis assumes close-range wireless transmission without significant channel delay spread between two nodes within the underwater network. For example, this work will be relevant to assessment and mitigation of inter-node interference within a network of underwater sensors where the direct arrival path between any two sensors significantly dominates over any multipath arrivals. As such, the proposed technique is applicable to freshwater closely spaced radio-frequency (RF) networks [23], but not so much within salt-water RF paradigm due to high conductivity of the medium [24]. Our method is also applicable to underwater acoustic networks with medium to long-range node spacing, where multipath scattering does not dominate the channel delay spread.

We now provide shallow water acoustic channel simulations using [22] for diverse oceanic conditions over medium and long ranges and discuss in each case the applicability of our technique to underwater acoustic networks. Specifically, we consider three scenarios in Figures 1-3: (i) shallow water depth (20 meters) medium-range (200 meters), (ii) shallow water depth (20 meters) long-range (1000 meters), and (iii) medium-water depth (60 meters) long-range (1000 meters). In each case, the transmitter and receiver were kept 10 meters from the ocean surface to examine the effect of multipath arrivals between the transmitter and receiver.

Figure 2.2 illustrates a channel simulation where the multipath interference is strong due to shortness of range (200 meters) and depth (20 meters), and therefore, not the intended paradigm for successful application of our method. On the other hand, multipath interference is drastically less in the simulated channel in Figure

2.3, which has same water depth but significantly longer range (1000 meters), which presents a well-suited case for successful application of our method. Finally, Figure 2.4 illustrates a simulated channel with greater water depth (60 meters) and long range (1000 meters) where the multipath arrivals are reduced in energy and manifest farther from the direct arrival in the channel delay spread. Our method may be directly applied to this channel after implementing an additional layer of real-time channel equalization.

The shallow water acoustic channel impulse response is closely shaped by the acoustic delay spread due to scattering of the transmitted acoustic energy by the ocean and reflections from the moving sea surface and static sea bottom. The lower-energy but persistent components of the channel delay spread, typical for shallow water medium ranges, are attributed mainly to environmental scattering, such as due to diffused reflections from the static sea bottom. The high-energy rapid channel fluctuations, which may pose significant interference to the direct arrival, are primarily due to specular reflections and focusing events [18] by the moving sea surface. As the range and water depth increases, greater acoustic scattering as well as increased absorption by multiple reflections results in less interference from multipath arrivals.

It is outside the scope of this work to provide specific channel estimation or equalization schemes, which are well-documented in the undersea signal processing and acoustic communications literature (refer e.g. [19; 21; 17] and references therein). Based on our discussion across case studies above, we will assume that the underwater network is deployed over a combination of water depths and ranges (e.g. Figures 2.3 and 2.4) where the interference from fluctuating multipath is either minimal or structured enough to be robustly compensated using popular equalization

techniques [21].

In the next chapter, the results of the system simulations will be shown. These are broken into two categories based on two very different underwater acoustic paradigms:

- Underwater acoustic channels where multipath interference is insignificant compared to the direct arrival: consider the multinode wireless system deployed in an acoustic channel similar to Figure 2.3, where the multipath arrivals are sufficiently scattered so that they contribute significantly less power than the direct arrival. An appropriate scenario corresponds to a long range underwater acoustic networks where the node-to-node channel is 1000 meter, possibly over depths of 20 meters or more to minimize sea floor reflections.

- Underwater acoustic channels where multipath interference is significant compared to the direct arrival: consider again the multinode wireless system deployed in a channel similar to Figure 2.4

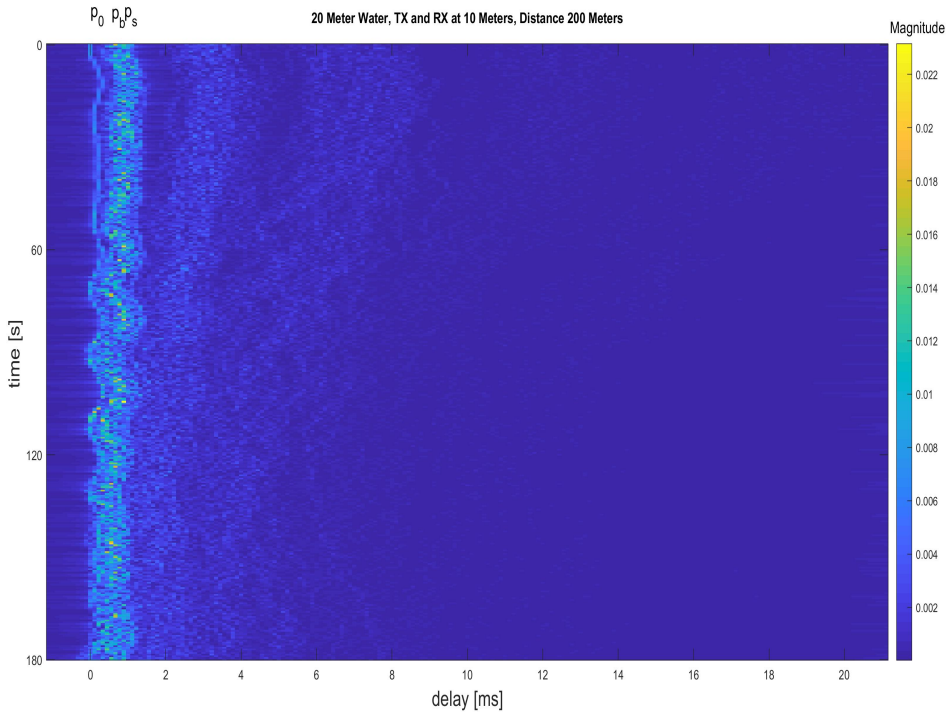

Figure 2.2: Simulated underwater acoustic channel with 20-meter water depth. The transmitter and receiver are set at 10-meters high at 200-meters apart. This simulates a shallow water scenario with significant interference due to reflections from the ocean surface or sea bottom. It is difficult to recover the direct-path signal in this situation because there are less reflections and thus the absorption of the signal is much less causing larger magnitude delay spread in the node-to-node channel.

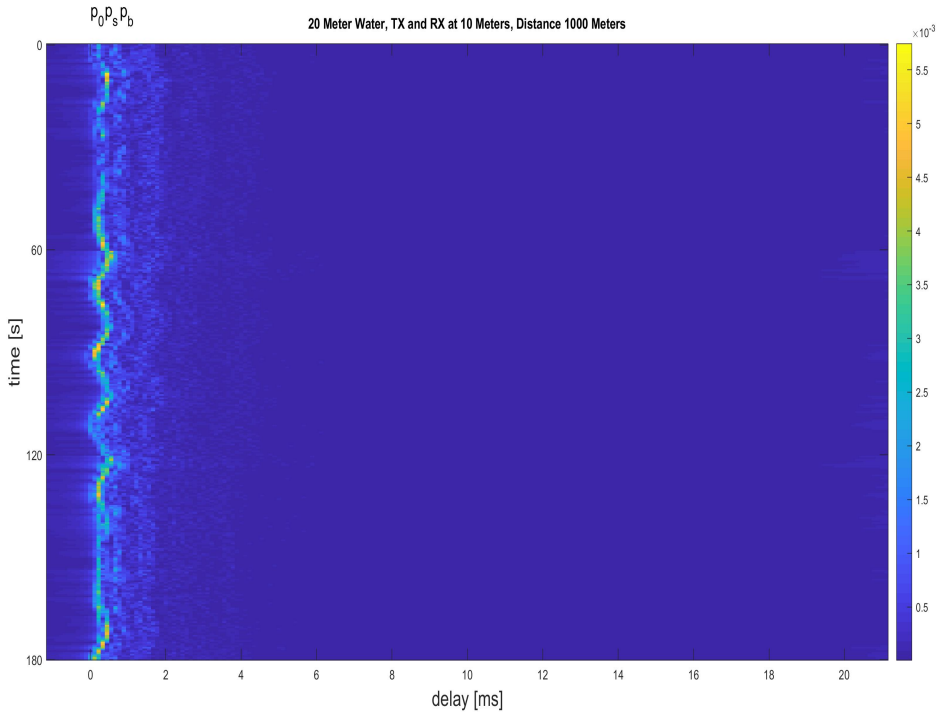

Figure 2.3: Simulated underwater acoustic channel with 20-meter water depth. The transmitter and receiver are set at 10-meters high at 1000-meters apart. This simulates a shallow water scenario with low multipath interference that is most compatible with our method, which is designed to mitigate node-to-node interference rather than multipath interference. Because of the shallow water depth and long-range distance between the transmitter and receiver, it takes longer and more reflections, and hence more energy absorption, for the multipath arrivals to reach the receiver.

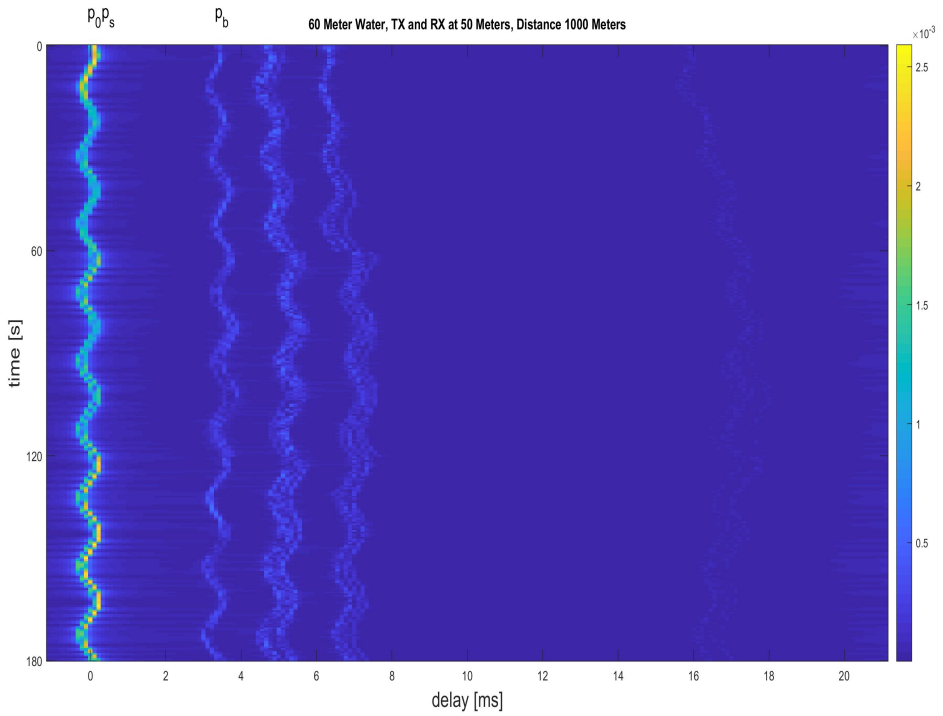

Figure 2.4: Simulated underwater acoustic channel with 60-meter water depth. The transmitter and receiver are set at 50-meters high at 1000-meters apart. This simulates a deep-water scenario with very weak and separable interference due to reflections from the surface or sea bottom.

CHAPTER 3
RESULTS

3.1 Performance Characterization

In [6], the simulation avoided a path loss model by assuming (unrealistically) that all destination nodes received sufficient SNR for perfect packet reception unless a packet experienced a collision with another packet transmitted from a node in the same received beam. Since realistic path losses would affect the conditions of a packet collisions, e.g. a packet collision due to a distant interfering transmitters may not cause enough interference to spoil the link with a closer transmitters, an interfering transmitters being within a beam-width is no longer a sufficient condition for a packet drop. Instead of the packet drop criteria from [6], we use SINR to help us determine the rate at which each transmitters can communicate reliably. We opt to use a fixed rate at which all the nodes are attempting to communicate, arbitrarily choosing 1 bit/channel use as the attempted communication rate. The criteria for a successful packet reception, then, by Shannon-Hartley theorem [13], is:

$$R_{MAX} = \frac{1}{2} log_2(1 + SINR) \geq 1 \tag{3.1}$$

The post-beamformed matched filter and post-beamformed partial decorrelator achievable rates can be calculated using Equations 2.18 and 2.30. The result of each of these equations is a vector of length N_s. We use these to determine if a packet is dropped or not in the following way: if any element in the vector is less than the desired rate of 1 bit/channel use, the packet is dropped. [1] Furthermore,

[1] We choose this criteria with the understanding that such a system could only be improved by

the receiver node must be in listening state for the entire packet duration for the packet to be possibly received.

An intelligent receiver is the one that first attempts to receive by matched filtering only, then if this fails, it attempts to use the MUD processing making sure only to include the interfering transmitters in the set $\mathbb{A}$. The other users, those in $\mathbb{B}$, are ignored by the MUD receiver and treated as noise. This intelligent receiver is labeled as MUD in our results and the matched filter alone receiver is labeled as MF.

3.2 MB-URAM Results

We re-ran the analysis in [6] for the case in which all packets are transmitted with the same power and the received power is determined using a realistic underwater signal attenuation model [16].[2] The simulation was performed for the case in which the nodes were distributed according to a two-dimensional spatial Poisson process with an average of N nodes per πr^2 circular area. All transmitted packets were done so with the same transmit power, packet duration time and idle duration time block lengths, but each transmitted packet had its own randomly chosen start time so that packets collided asynchronously at any given receiver.

The results of this simulation are summarized in Figure 3.1 where we show the central node's average throughput as a function of the total number of nodes in the network for three different values of x. We see a similar trend in that the throughput is maximized when there are 4 to 6 nodes randomly spatially distributed within the 100 m radius network. We also notice the effect of packet transmission

implementing an error correcting code. For this reason, the results here can be seen as an informal lower bound on performance.

[2]In the future work, we recommend characterization include the effect of adding power control techniques.

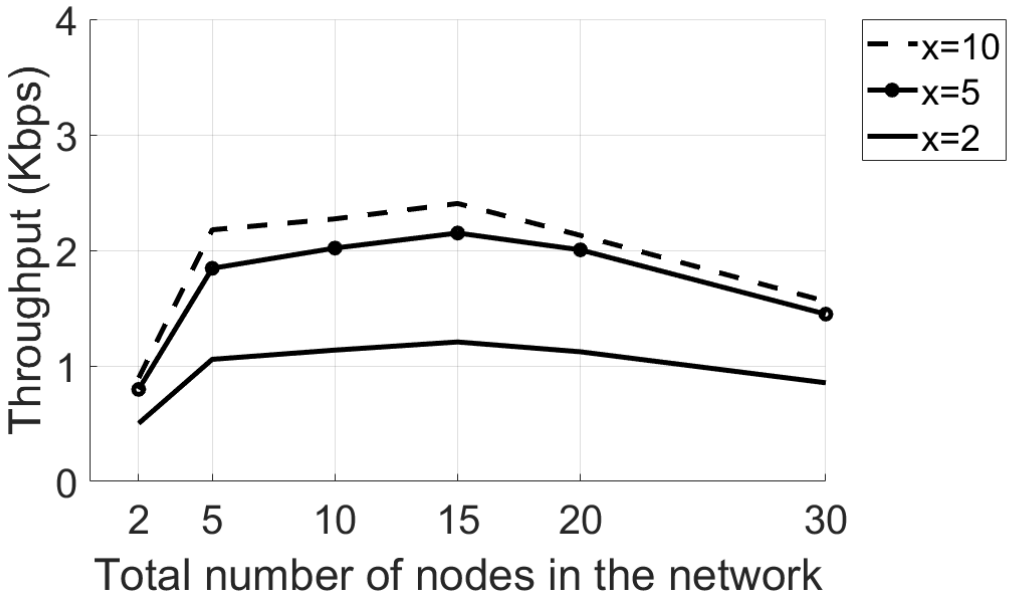

Figure 3.1: Central nodes average throughput of MB-URAM with the matched filter receiver. From [6] we know that the parameter x ultimately limits the throughput by (x-1)/x. That is, for x=10 the best MB-URAM can achieve is 90% of the maximum throughput. But, with realistic power loss and interference introduced here, we see that the throughput is instead limited by increasing number of nodes in the network. This simulation is for SNR = 5 dB, 20 symbols per packet, 1 chip per symbol, 4 transducers, and allowing a single packet to be transmitted at a time.

frequency that is governed by the parameter x.

3.3 MAMBU-RAM Results

For the simulation, we examine the number of successfully received packets for the centrally located node. We show results for different signature signal spreading lengths (e.g. we vary the number of chips/symbol from 1-16 chips/symbol). Each of the plots were generated by 100 runs where each run consisted of laying out the nodes and elapsing 100 time slots, with each transmitted packet consisting of 20 symbols. For the various plots produced, it is important to realize that the matched filter is being performed after the beam-gain is applied and likewise the decorrelator MUD is performed in the same way. The SNR is the signal to noise ratio without any interference present. We simulate for $SNR = 5$ dB, where SNR is the SNR of the weakest transmitter (farthest transmitter from the centrally located receiver). Since all nodes transmit packets at the same transmit power, nodes that are closer to the centrally located receiver under examination will benefit from a higher SNR.

Figure 3.2 shows results for a network with 4-nodes and allowing the transmitting node to send a single packet at a time. Four solid curves are shown for the matched filter post-beam receiver (MB-URAM) and four dashed curves for the decorrelator post-beam receiver (MAMBURAM). The MAMBURAM curves show significant increases over the MB-URAM counterparts. Specifically, the maximum throughput values for MAMBURAM are significantly higher than for MB-URAM, and the throughput drops off less quickly as the number of nodes is increased. This behavior is the result of the decorrelating detector's ability to successfully receive packets even when more than one transmitter is located in a single receive beam and packets collide.

Although the results in Figure 3.2 show that MUD nodes perform better than the MF nodes for keeping the chips per symbol the same. However, we never see when can additional chips benefit you. For this, we allow each transmitter send two simultaneous beams at the same time, where each chooses a signature sequences so that they are orthogonal if possible (orthogonal beams is not possible for the 1 cps case). In Figure 3.3, we see that the additional transmit beam severely degrades the performance of the single chip per symbol curve whereas the multiple chips cases are far less affected since they are able to choose orthogonal sequences.

Notice that even for the unspread case (a single chip per symbol), the decorrelator (MAMBURAM) enables a small improvement over the matched filter (MB-URAM) for the moderately dense networks with four to six nodes. The improvement is due to the decorrelator's ability to partially null out interference in the time domain that is enabled by the natural symbol timing offsets between the different transmissions.[3]

The results shown in Figure 3.2 and 3.3 motivate the use of MAMBURAM over MB-URAM while revealing two design factors for consideration. There exists a well known spreading-throughput trade in which a throughput degradation is caused by "slowing down" the signal by concatenating more chips per symbol.[4] The decorrelator, however, is designed to take maximum advantage of the signal differences created by the longer chip signature sequences.

Looking more closely at the Figure 3.3 for the case of more than 15 nodes in the network, we see that additional chips become necessary along with MUD as the single chip systems receivers are no longer able to out perform the 4 chips/symbol

[3]For the unrealistic case of all received packets being completely symbol synchronous, the decorrelator would break down since the inverse of $\mathbf{R}$ would not exist.

[4]Note that we have constrained the system bandwidth to be constant and therefore achieve a spreading gain of direct spread spectrum by concatenating more chip pulses in time.

MUD receiver despite the fact that each packet is now taking four times as long to send. For example, a system with 4 transducers and an expected node density of $\frac{15 \text{ nodes}}{\pi 100^2}$ square meters would be best served operating with 4 chips per symbol. Likewise, if the density becomes lesser than $\frac{15 \text{ nodes}}{\pi 100^2}$ square meters then the MUD with 1 chip per symbol is advised.

These results motivate the design of any MAMBURAM system to be waveform adaptive so as to reap the benefits of the decorrelator without suffering the throughput degradation that is caused by using more chips/symbol that is required. Ideally, such a waveform-adaptive MAMBURAM system would provide a throughput curve equivalent to the maximum of all the curves shown in the figure.

The effect of varying the number of transducers is shown in Figure 3.4. As the number of transducers increases, the beamwidth becomes narrower and both MB-URAM and MAMBURAM nodes are more easily able to form links between each other while limiting interference from other nodes. In agreement with the findings from [6] Figure 3.4 shows that adding transducers to a single chip system improves performance. The drawback of adding more transducers to each node is that many systems are size-weight-and-power (SWaP) constrained and simply will not accommodate additional transducers. SWaP constrained nodes will benefit from using the MUD receiver in place of the matched filter receiver.

In Figure 3.5 we examine how additional transducers can benefit either receiver model. This figure shows the central node's average throughput versus the number of nodes in the network for varying number of transducers. With less transducers, the achievable beam width grows allowing more interference to cause dropped packets as more users are introduced into the network. The figure emphasizes that while the MUD aided receiver achieves higher throughput throughout, both will benefit

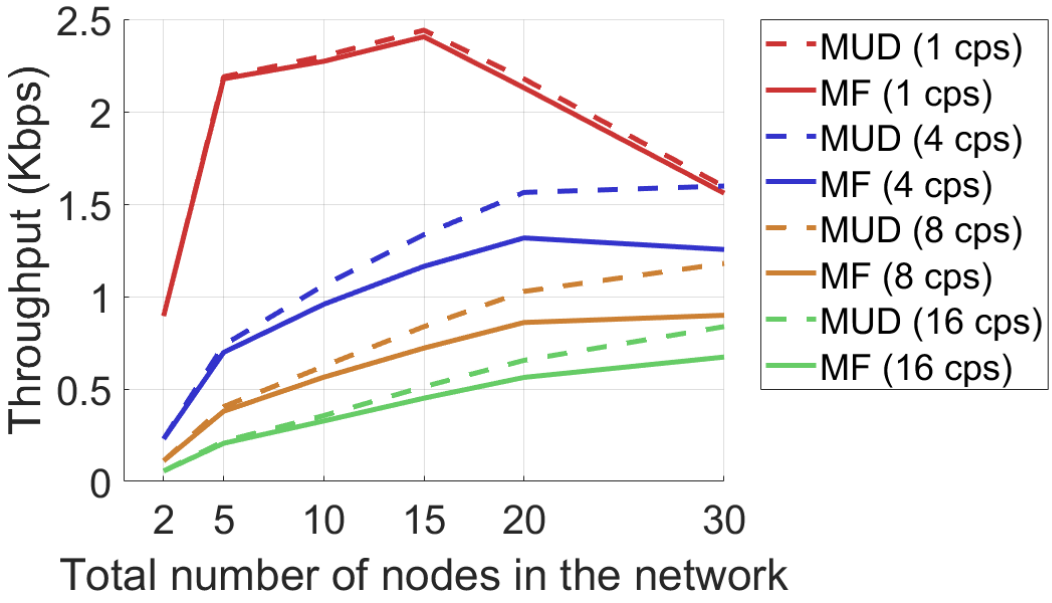

Figure 3.2: Effect of varying the number of chips per symbol (cps) on the central nodes average throughput. As the number of nodes in the network increases, we see the MUD receivers outperforming the MF for the same number of cps. Further, for more than 20 nodes in the network, we see that the 16 cps MUD is greater than the 8 cps MF and at 30 nodes the 8 cps MUD matches the 4 cps MF receiver. But throughout, it is the 1 cps MF is still greater than any MUD with > 1 cps. This simulation is for SNR $= 5$ dB, x $= 10$, packet size of 20 symbols, 4 transducers, chip rate of 4 Kcps, transmitting one packet at a time, and varying the number chips per symbol.

from the addition of more transducers leading to a more effective spatial matched filtering. It can be seen that additional transducers can, in each case shown, be effectively replaced by performing the MUD based receiver described in this paper. The MUD receiver with 2 less transducers traces very closely the MF receiver with additional transducers. This result suggests that MAMBURAM system may be suitable to SWaP constrained nodes as previously mentioned.

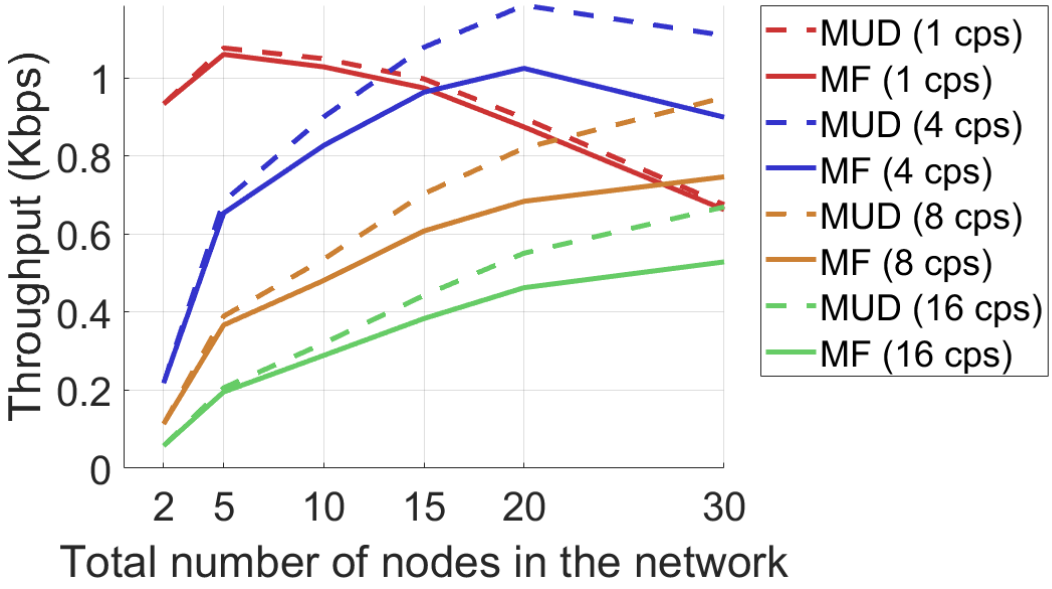

Figure 3.3: Effect of varying the number of chips per symbol (cps) on the central nodes average throughput while allowing transmitting nodes to send two simultaneous packets. In all cases, we see that allowing simultaneous packets to be sent decreases the throughput compared to the single packet transmitting case in Figure 3.2. It is important to note that the additional chips per symbol makes the decrease in performance less severe. The 1 cps system suffers greatly, but the 4 cps system experiences less of a decrease and past 15 nodes in the network, we see the 4 cps MUD outperforming all others. This simulation is for SNR = 5 dB, x = 10, packet size of 20 symbols, 4 transducers, chip rate of 4 Kcps, transmitting two simultaneous packets at a time, and varying the number chips per symbol.

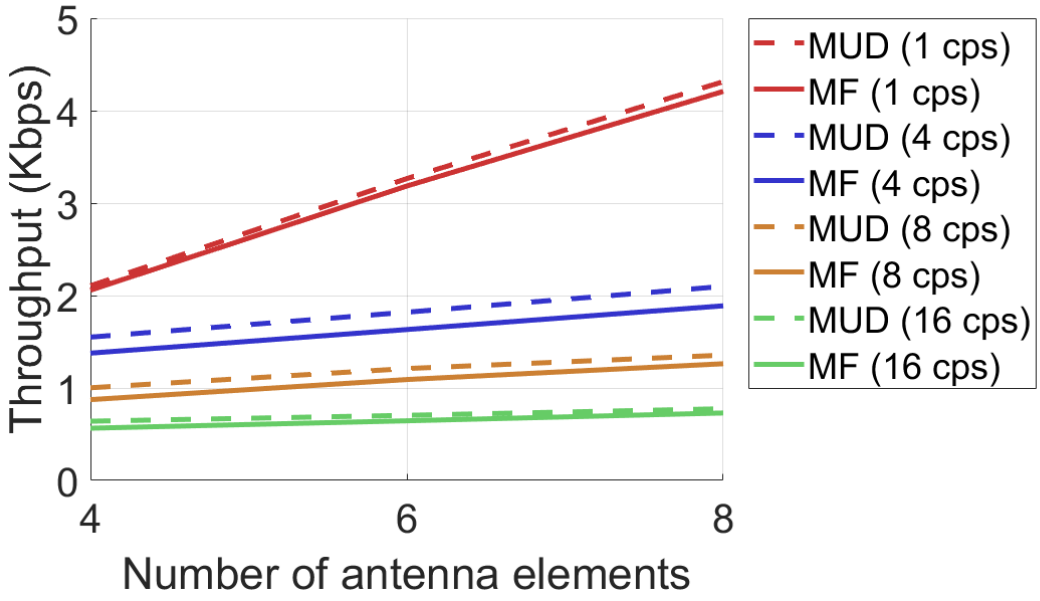

Figure 3.4: Effect of varying number of transducers on the central node's average throughput. For systems with higher number of transducers the beamwidth will be narrower and be better able to discriminate between tightly spaced transmitters. The system with 1 cps stands to benefit the most from additional transducers. This simulation was for a $SNR = 5$ dB, x = 10, packet size of 20 symbols, 4 chips per symbol, and variable number of transducers. The network area is $\pi 100^2$ square meters.

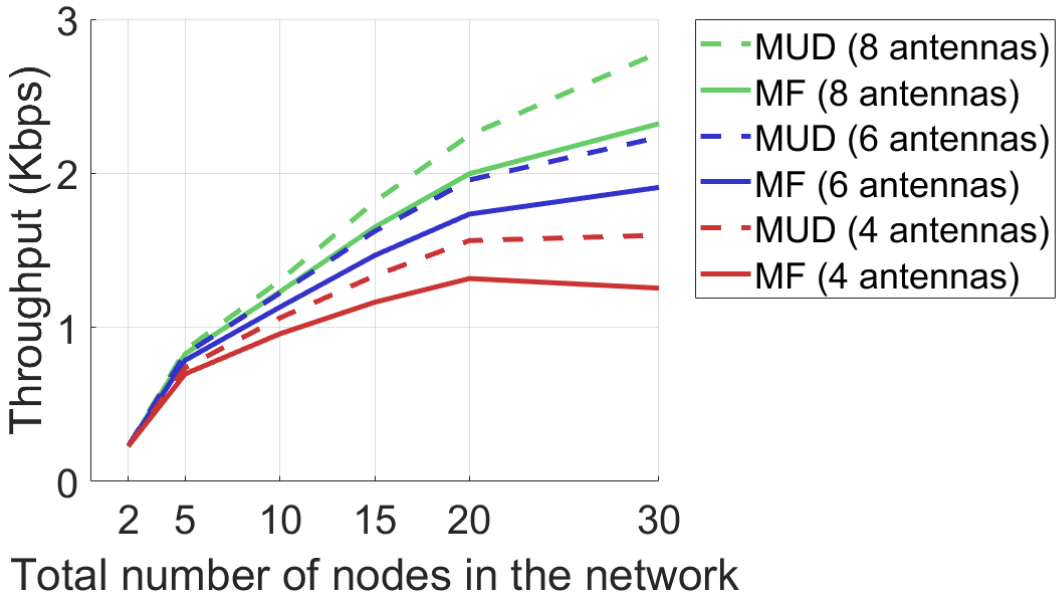

Figure 3.5: Effect of varying the number of transducers on the central nodes average throughput. As the number of transducers is increased, a node will form a narrower beam giving an increased ability to discriminate between tightly spaced transmitters. Based on this figure, it can be seen that an additional 2 receive elements gives approximately the same increase in throughput as the MUD decorrelating receiver. For example, the MUD receiver with 4 transducers traces the curve of the MF receiver with 6 transducers. This simulation is for SNR = 5 dB, x = 10, packet size of 20 symbols, 4 transducers, 4 chips per symbol, chip rate of 4 Kcps, transmitting one simultaneous packet at a time, and varying the number chips per symbol.

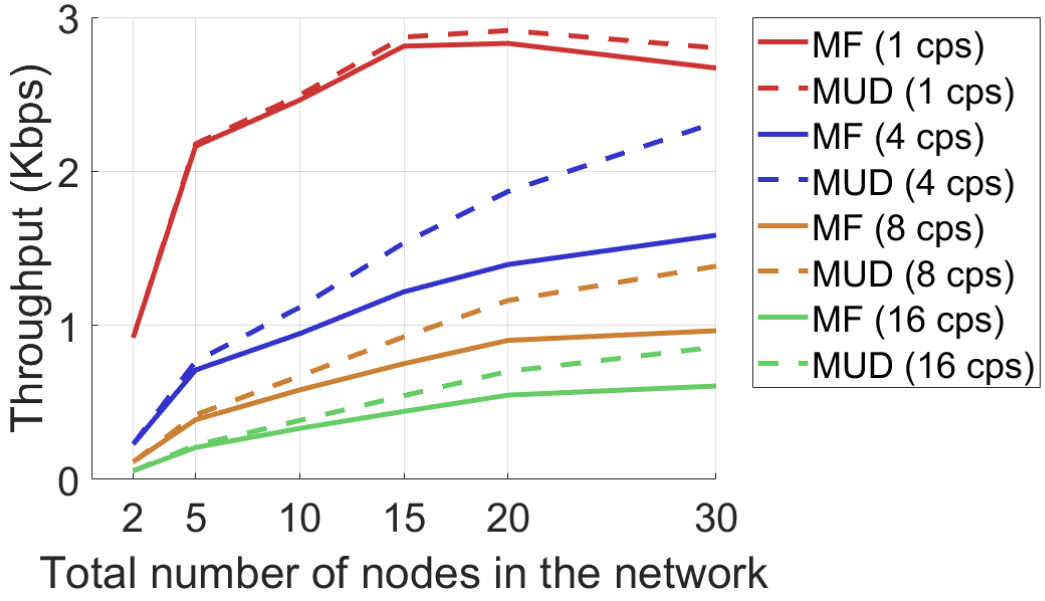

Figure 3.6: Effect of varying the number of chips per symbol (cps) on the central nodes average throughput. This simulation is for SNR = 5 dB, x = 10, packet size of 20 symbols, 4 transducers, chip rate of 4 Kcps, transmitting one packet at a time, path loss of $\frac{1}{r^3}$, and varying the number chips per symbol.

3.4 Underwater Channel

For the underwater channel, propagation physics are vastly different for that of a typical over-the-air RF system due its dynamic nature. But for such channels where the direct arrival component is strong compared to the multi-path reflections, a simple power loss model can also be adopted using a $\frac{1}{r^3}$ attenuation [26]. In Figures 3.6, 3.7, 3.8, and 3.9, the results for such a system are presented using the $\frac{1}{r^3}$ path loss.

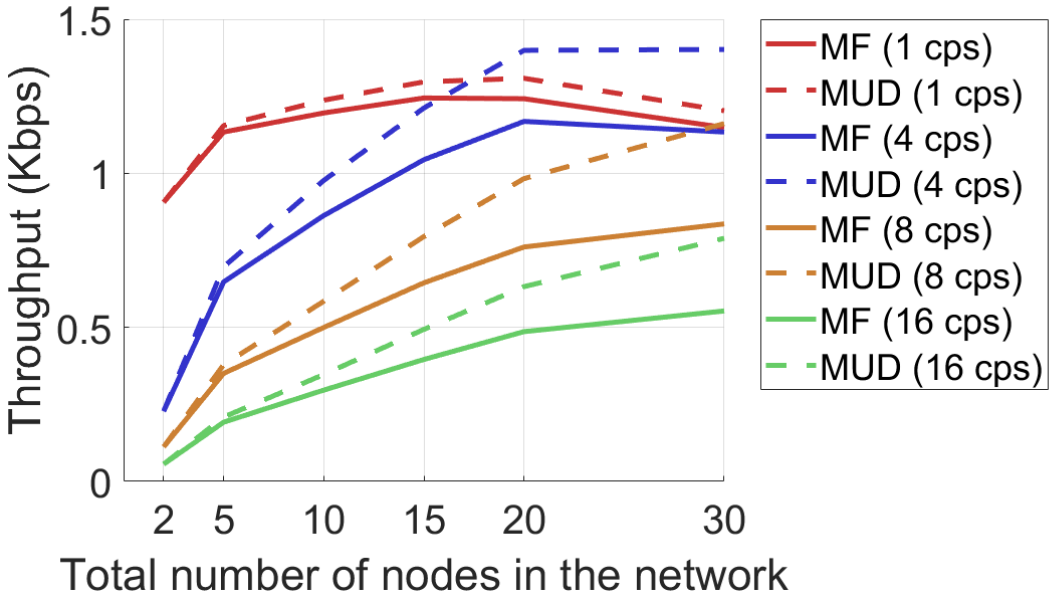

Figure 3.7: Effect of varying the number of chips per symbol (cps) on the central nodes average throughput while allowing transmitting nodes to send two simultaneous packets. This simulation is for SNR = 5 dB, x = 10, packet size of 20 symbols, 4 transducers, chip rate of 4 Kcps, transmitting two simultaneous packets at a time, path loss of $\frac{1}{r^3}$, and varying the number chips per symbol.

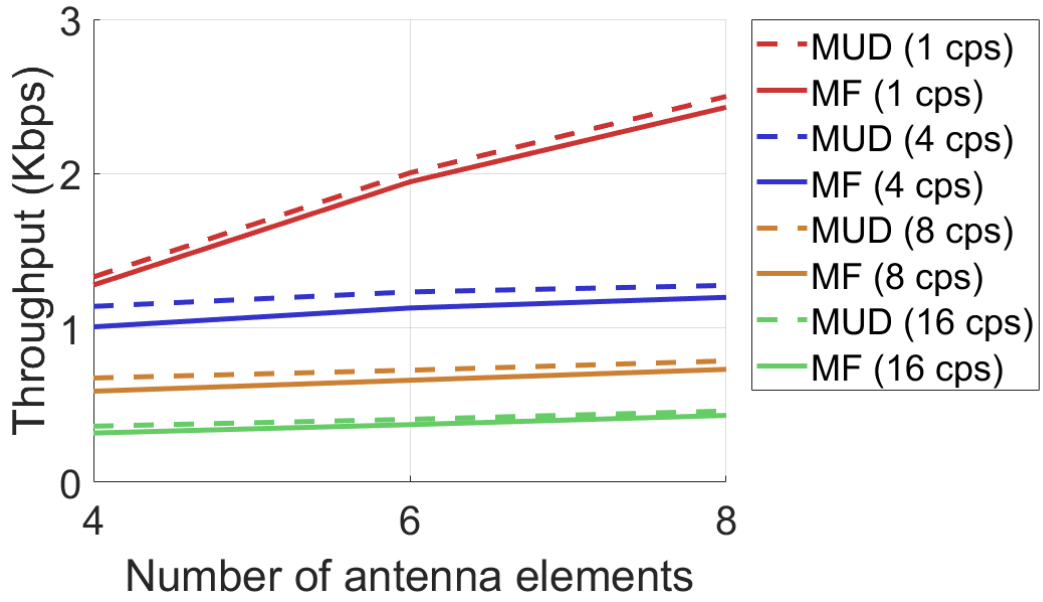

Figure 3.8: Effect of varying number of transducers on the central node's average throughput. For systems with higher number of transducers the beamwidth will be narrower and be better able to discriminate between tightly spaced transmitters. This simulation was for a $SNR = 5$ dB, x = 10, packet size of 20 symbols, 4 chips per symbol, transmitting one beam at a time, path loss of $\frac{1}{r^3}$, and variable number of transducers. The network area is $\pi 100^2$ square meters with 10 nodes.

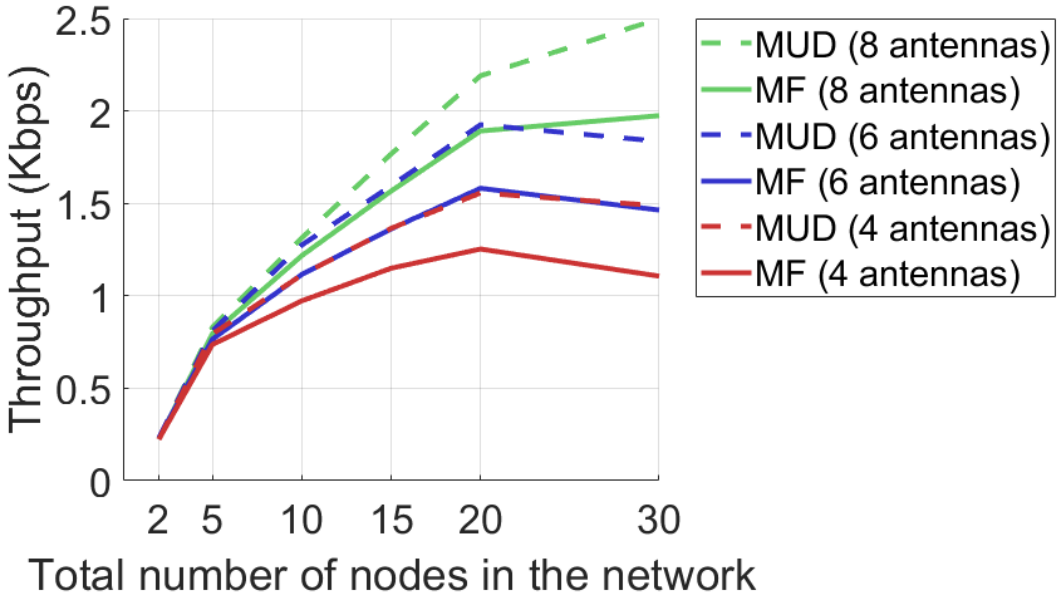

Figure 3.9: Effect of varying the number of transducers on the central nodes average throughput. As the number of transducers is increased, a node will form a narrower beam giving an increased ability to discriminate between tightly spaced transmitters. This simulation is for SNR = 5 dB, x = 10, packet size of 20 symbols, 4 transducers, 4 chips per symbol, chip rate of 4 Kcps, transmitting one simultaneous packet at a time, path loss of $\frac{1}{r^3}$, and varying the number chips per symbol.

3.5 Underwater Channel Equalization

A decorrelating detector can be used to mitigate interference by nulling out unwanted signals. Another application of this type of receiver is to eliminate interference caused by multi-path components. The underwater communication channel is a dynamic environment and a signal propagating undergoes reflections from both the sea floor as well as the ever changing sea surface. For our analysis, a realistic underwater channel was generated by using the Bellhop model [25]. We simulate for a simple two node scenario with a three tap channel impulse response (CIR). The setup is illustrated in Figure 3.10. The magnitude plot of the underwater channel used is included in Figure 3.11. It can be seen that the direct arrival is at a constant delay with strong gain and the multi-path components are weak with varying delays. From the results in Figure 3.12 we see that the throughput performance converges for large number of chips per symbol (16 chips per symbol). The additional chips being added to the signature sequence is causing the cross-correlations to be less which means that the multi-path components will leak through the direct signals less due to combination of timing offset and additional chips.

We define link outage probability to be one minus the number of successful receptions divided by the number of reception attempts: $P_{\text{outage}} = 1 - \frac{N_{sr}}{N_{ar}}$, where N_{sr} and N_{ar} are the number of successful receptions and number of attempted receptions respectively. In Figure 3.13 we see that the link outage probability for a single chip matched filter system is very high. Such a system would prove to practically unusable. For this reason it is advisable to introduce more chips again to decrease the cross-correlations such that the matched filter and decorrelating receiver begin to mimic each other as these values decrease.

In Figure 3.14 the cross-correlation matrix, $\mathbf{R}$, is shown for varying number

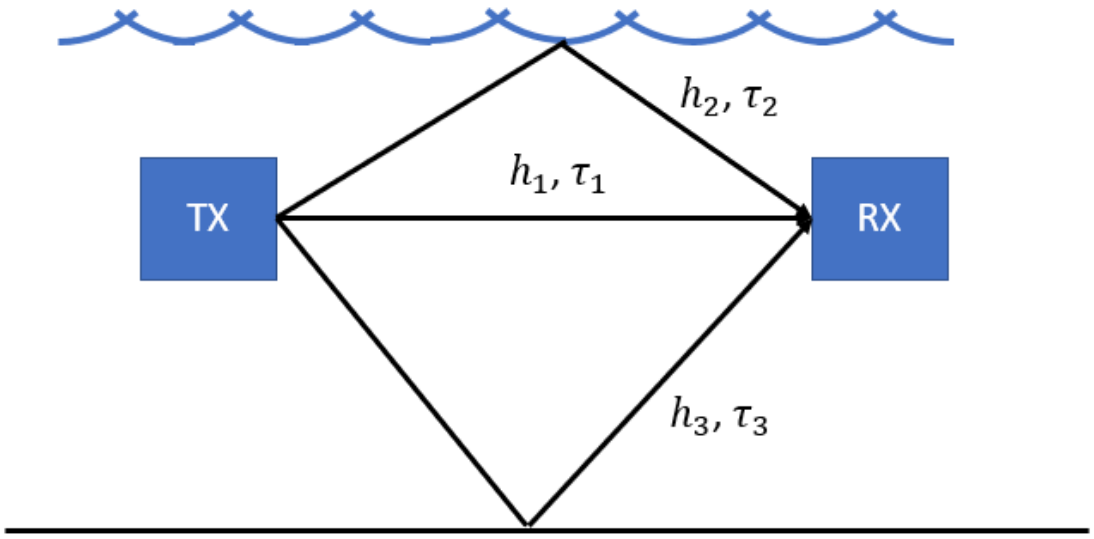

Figure 3.10: Underwater channel equalization simulation setup. A realistic three tap underwater channel was generated to obtain the parameters. The noise variance was calculated by the residual power in the channel after taking the channel taps into account.

of chips per symbol. As the number of chips per symbol increases the packets take longer to send and more overlap may occur. However, because of the timing offsets and the signature sequence is randomly generated, the correlations become smaller while the matrix begins to approach an identity matrix (ie. the users are orthogonal). In this limiting case, the traditional matched filter and decorrelating receiver will perform similarly as we have discussed in the previous figures of throughput and link outage probability.

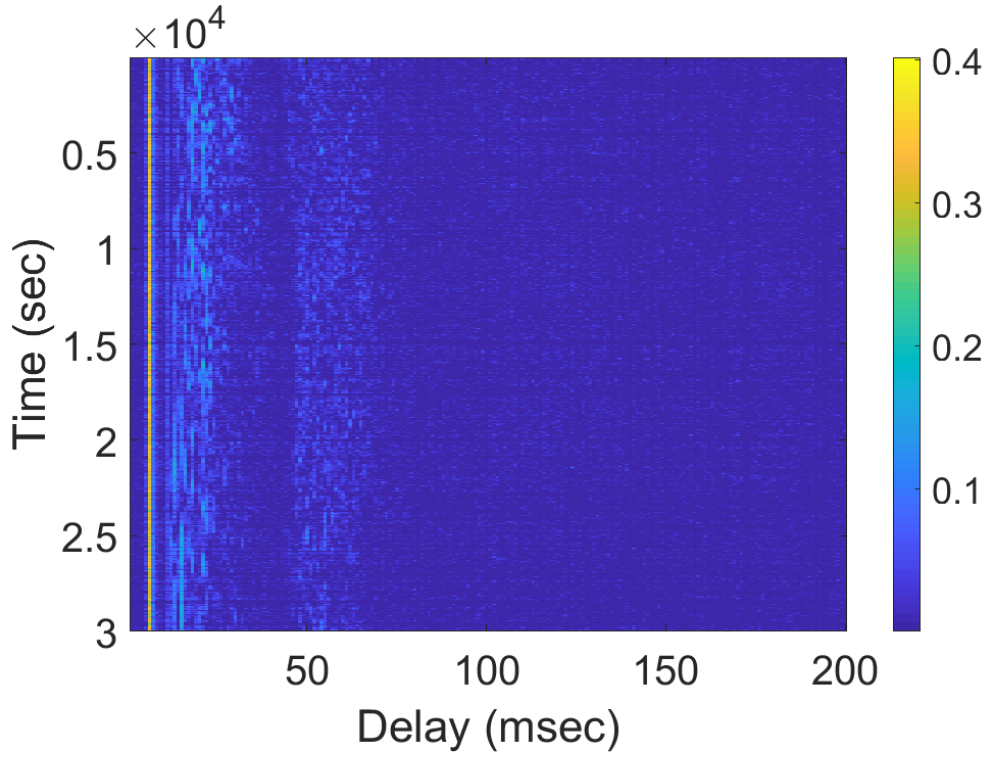

Figure 3.11: Magnitude of the underwater multi-path channel used in the simulation. We deconstructed this into a three tap channel (direct arrival and two multi-path components) and the rest of the energy in the channel is used to compute the noise variance for the AWGN added at the receiver. It can be seen that the direct arrival path is approximately constant delay and strong gain.

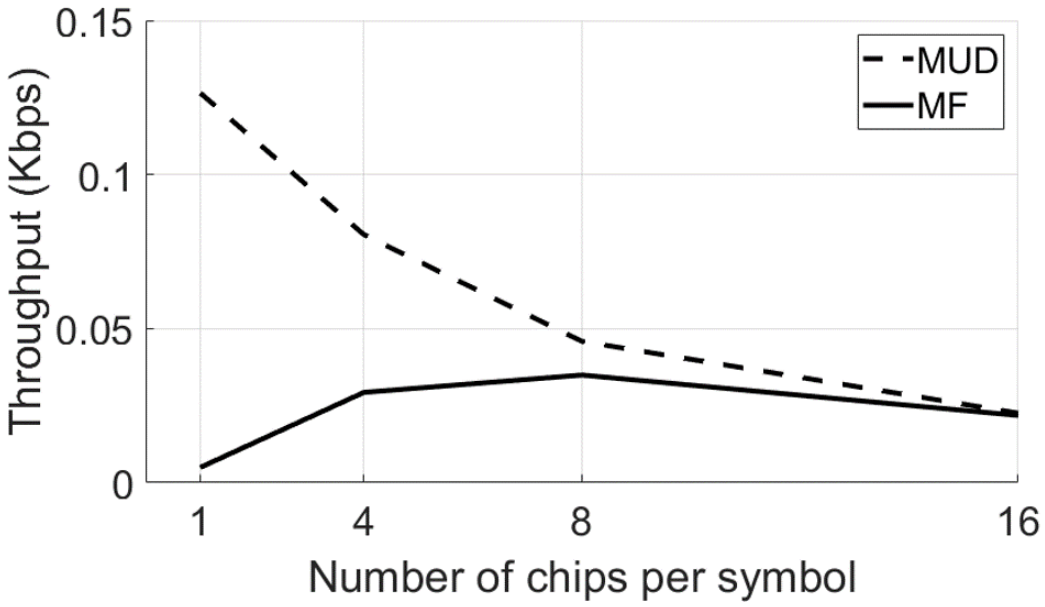

Figure 3.12: MAMBU-RAM underwater channel equalization throughput results. Performance converges for large number of chips per symbol due to the cross-correlation matrix approaching identity. This simulation was done using the realistic underwater channel described above.

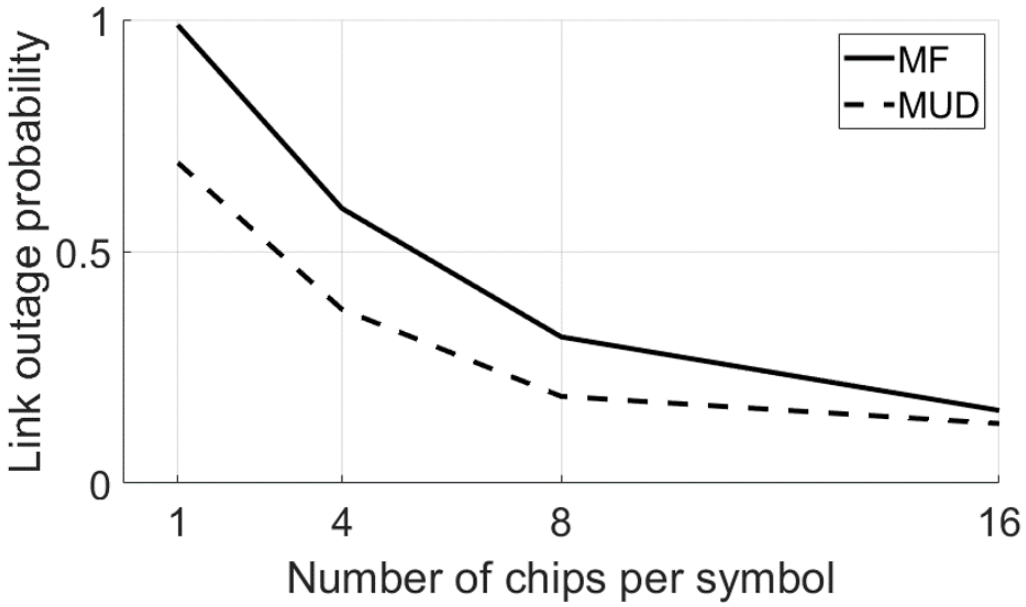

Figure 3.13: MAMBU-RAM underwater channel equalization link outage probability results. At 1 cps, it can be seen that the traditional matched filter is almost always failing to complete a successful transmission due to multi-path components overlapping significantly in time and strong correlations between these components and the direct arrival. Increasing the number of chips per symbol, forces the correlations to decrease since the randomness in the signature sequence decreases the off-diagonal values in the cross-correlation matrix. Performance converges for MF and MUD for large number of chips per symbol.

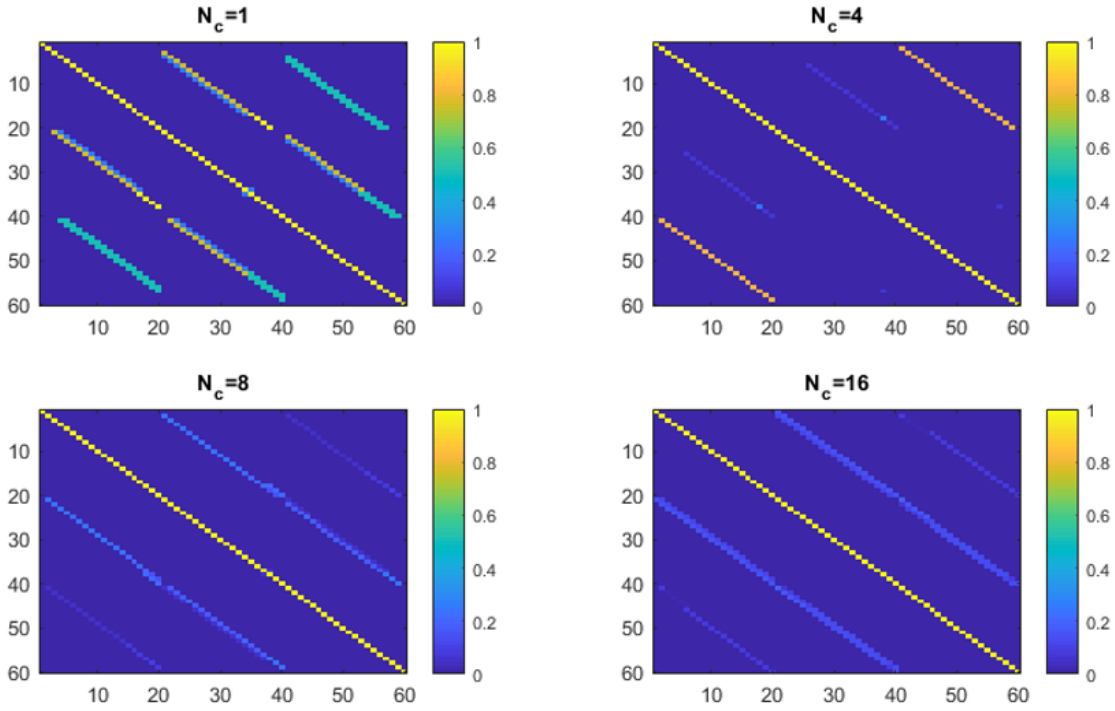

Figure 3.14: Cross-correlation matrix for the MAMBU-RAM underwater channel equalization simulation for varying number of chips per symbol. It can be seen that for more chips per symbol the correlation matrix off-diagonal elements values decreases and the matrix begins to approach identity. Indeed, this is the reason that for increasing chips the performance of the traditional matched filter and decorrelator converges in the above two plots of throughput and link outage probability.

CHAPTER 4
CONCLUSION

In this paper, we reviewed a Multi-Beam Uncoordinated Random Access MAC (MB-URAM) for digital beamforming systems. It was shown through numerical simulations that for a fixed communication rate, packet drops become prohibitive in dense node environments when limited number of receive elements are unable to null out interference. We proposed the use of a linear multiuser detector at each of the nodes, namely the decorrelating detector after the beamformer, to lessen the packet drops by nulling out interfering signals. Our analysis demonstrates that when a decorrelating detector is implemented, the link throughput is improved. An underwater channel equalization scheme was introduced which utilizes the MUD receiver to null out the multi-path interference and a simulation was done using a realistic underwater channel which showed improvements can be made in both throughput and link outage probability while using the MUD receiver and justifications were given by comparing cross-correlations.

Future directions of research include repeating the study for nodes with circular and other advantageous receive element positioning, as well as adding layers of complexity to both the MB-URAM and MAMBU-RAM systems such as of power control, additional types of MUD receivers, ie. optimal MUD and/or successive interference cancellation (SIC), different network topologies, allowing for random packet arrivals at the transmitter, more advanced adaptive digital beamforming algorithms, and different beam selection algorithms. For the algorithms that would

require estimation of received signal parameters such as relative timing of the received colliding packets, the effects of signal estimation error on throughput should be studied, as well.

CHAPTER 5
BIBLIOGRAPHY

[1] D. Tse, P. Viswanath, *Fundamentals of Wireless Communication*. Cambridge University Press, 2005.

[2] J. Litva, T. K. Lo, *Digital beamforming in wireless communications*. Artech House, Inc., 1996.

[3] B. D. Van Veen, K. M. Buckley, "Beamforming: A versatile approach to spatial filtering", *IEEE assp magazine*, vol. 5, no. 2, pp. 4-24, 1988.

[4] Zhensheng Zhang, "Pure directional transmission and reception algorithms in wireless ad hoc networks with directional antennas," *IEEE International Conference on Communications*, 2005. ICC 2005. 2005, 2005, pp. 3386-3390 Vol. 5.

[5] A. E. Sayers, W. M. Dorsey, K. W. O'Haver, J. Valenzi *et al.*, "Planar near-field measurement of digital phased arrays using near-field scan plan reconstruction", *Antennas and Propagation, IEEE Transactions on Antennas and Propagation*, vol. 60, no. 6, 2012.

[6] G. Kuperman, R. Margolies, N. M. Jones, and A. Narula-Tam, "Uncoordinated MAC for Adaptive Multi-Beam Directional Networks: Analysis and Evaluation", *2016 25th International Conference on Computer Communication and Networks (ICCCN)*, 2016.

[7] S. Verdu, *Multiuser Detection*. Cambridge University Press, 1998.

[8] R. Lupas and S. Verdu, "Linear multiuser detectors for synchronous code-division multiple-access channels," in *IEEE Transactions on Information Theory*, vol. 35, no. 1, pp. 123-136, Jan 1989.

[9] R. Lupas and S. Verdu, "Near-Far Resistance of Multiuser Detectors in Asynchronous Channels", in *IEEE Transactions on Communications*, vol. 38, no. 4, pp. 496-508, April 1990.

[10] A. Duel-Hallen and C. Heegard, "Delayed decision-feedback sequence estimation," in *IEEE Transactions on Communications*, vol. 37, no. 5, pp. 428-436, May 1989.

[11] D. Tse and S. Hanly, "Linear Multiuser Receivers: Effective Interference, Effective Bandwidth and User Capacity", in *IEEE Transactions on Information Theory*, vol. 45, no. 2, pp. 641-657, March 1999.

[12] P. Xiong, I. N. Psaromiligkos, and S. N. Batalama, "On the Relative Output SINR of Full and Partial Decorrelators", in *IEEE Transactions on Communications*, vol. 51, no. 10, pp. 1633-1637, October 2003.

[13] T. M. Cover, J. A. Thomas, *Elements of Information Theory (Wiley Series in Telecommunications and Signal Processing)*. John Wiley & Sons, Inc., 2001.

[14] G. Strang, *Introduction to Linear Algebra,* 5^{th} *Edition*. Wellesley-Cambridge Press. 2015.

[15] U. M. Qureshi, F. K. Shaikh, Z. Aziz, S. M. Z. S. Shah, A. A. Sheikh, E. Felemban, and S. B. Qaisar, "RF Path and Absorption Loss Estimation for Underwater Wireless Sensor Networks in Different Water Environments", in *Sensors*, 16, 890, 2016.

[16] B. Ehlers, A. Sen Gupta, and R. McCarthy, "Multi-Beam Uncoordinated Random Access MAC for Underwater Communication Networks", in ACM International Workshop on UnderWater Networks (WUWNet), Dec. 2018.

[17] M. Stojanovic and J. Preisig, "Underwater acoustic communication channels: Propagation models and statistical characterization", in *IEEE Communications Magazine*, vol. 47, no. 1, pg. 84-89, 2009.

[18] J. Preisig and G. Deane, "Surface wave focusing and acoustic communications in the surf zone", in *The Journal of the Acoustical Society of America*, vol. 116, no. 4, pg. 2067-2080, 2004.

[19] A. Gupta and J. Preisig, "A geometric mixed norm approach to shallow water acoustic channel estimation and tracking", in *Physical Communication*, vol. 5, no. 2, pg. 119-128, 2012.

[20] A. Gupta and A. Williams, "Mitigating the effect of multipath interference in shallow water acoustic channels", in *Ocean Electronics (SYMPOL)*, pg. 1-4, 2013.

[21] M. Stojanovic, J. Proakis, and J. Catipovic, "Performance of high-rate adaptive equalization on a shallow water acoustic channel", in *The Journal of the Acoustical Society of America*, vol. 100, no. 4, pg. 2213-2219, 1996.

[22] P. Qarabaqi and M. Stojanovic, "Statistical characterization and computationally efficient modeling of a class of underwater acoustic communication channels", in *IEEE Journal of Oceanic Engineering*, vol. 38, no. 4, pg. 701-717, 2013.

[23] F. Teixeira, P. Freita, L. Pessoa, R. Campos, and M. Ricardo, "Evaluation of IEEE 802.11 Underwater Networks Operating at 700 MHz, 2.4 GHz and 5 GHz", in *Proceedings of the International Conference on Underwater Networks & Systems*, pg. 11, 2014.

[24] A. Shaw, AI. Al-Shamma'a, S. Wylie, and D. Toal, "Experimental investigations of electromagnetic wave propagation in seawater", in *2006 European Microwave Conference*, pg. 572-575, 2006.

[25] M. Porter and YC. Liu, "Finite-Element Ray Tracing", in *Theoretical and Computational Acoustics*, vol. 2, pg. 947-956, 1994.

[26] UM. Qureshi, FK. Shaikh, Z. Aziz, SM. Shah, AA. Sheikh, E. Felemban, and SB. Qaisar, "RF Path and Absorption Loss Estimation for Underwater Wireless Sensor Networks in Different Water Environments", in *Sensors*, vol. 16, no. 6, 2016.